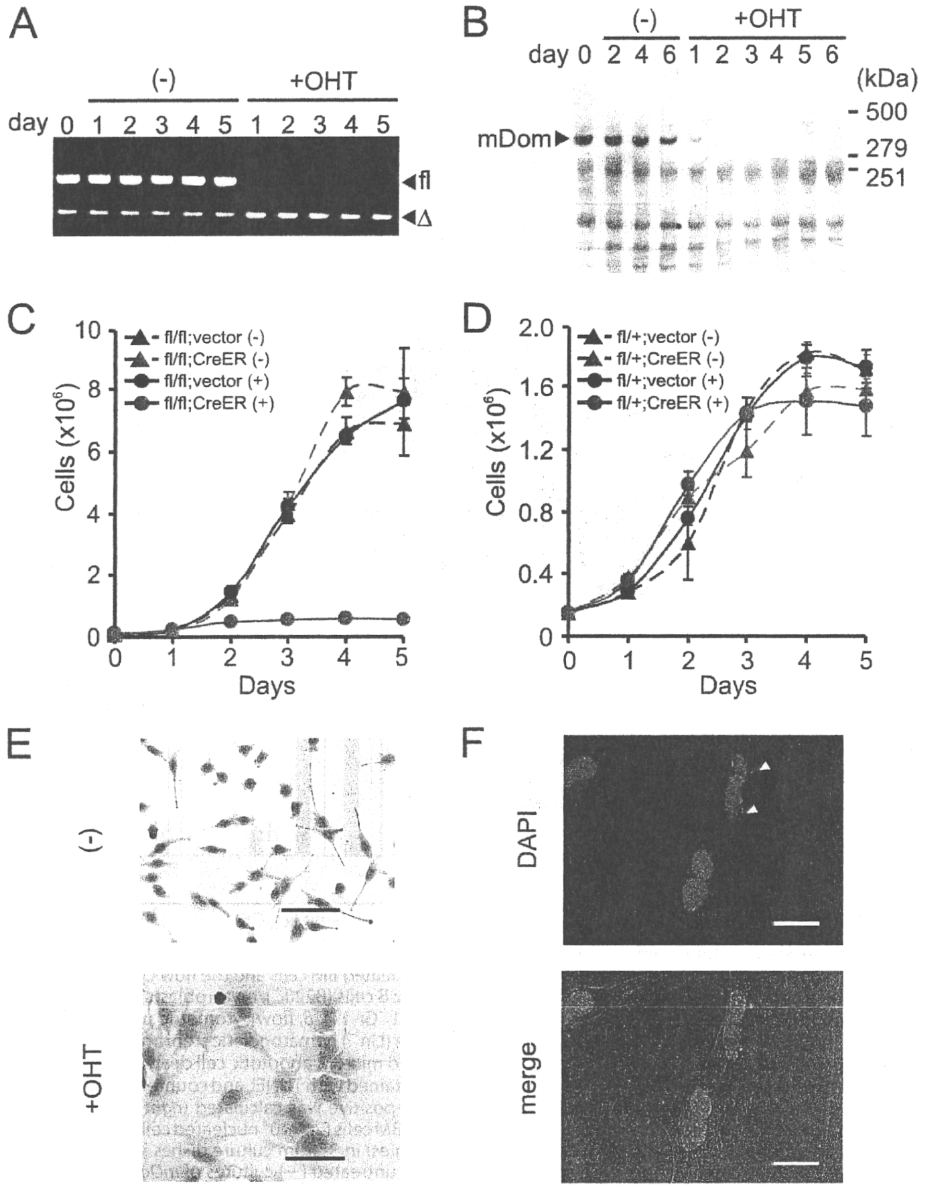

FIGURE 4. **Strong growth inhibition of conditional mDomino-deficient embryonic fibroblasts.** *A*, PCR analysis of the *mDom*^{fl} deletion by OHT. *mDom*$^{fl/fl}$*;CreER* MEFs were left untreated (−) or treated with 7.5 nM OHT for 8 h, washed and further cultured, and then analyzed for the status of the *mDom*^{fl} allele on the indicated days. *B*, Western blot analysis of the mDomino protein in the whole cell lysate of *mDom*$^{fl/fl}$*;CreER* MEFs treated with OHT. *C* and *D*, growth defect of mDomino-deficient MEFs. Four types of retrovirally transduced MEF lines, *mDom*$^{fl/fl}$*;CreER* (*left*), *mDom*$^{fl/+}$*;CreER* (*right*), and their respective vector controls, were left untreated (−) or treated with OHT (+), and then cultured in the normal medium. At the indicated times, the cells were trypsinized and counted. Data are the means ± S.D. of three separate experiments. *E* and *F*, nuclear abnormalities observed in mDomino-deficient MEFs. *E*, Wright-Giemsa staining of the OHT-treated or untreated (−) *mDom*$^{fl/fl}$*;CreER* MEFs after 6 days of culture. *Scale bars* represent 100 μm. *F*, DAPI staining of OHT-treated *mDom*$^{fl/fl}$*;CreER* MEFs (*upper*). *Arrowhead* indicates cells with micronuclei. The DAPI image is *merged* with its bright-field image (*lower*). *Scale bars* represent 25 μm.

tion in the colony formation of the *mDom*$^{\Delta/fl}$*;Mx1-Cre* cells (Fig. 3*F*, *right*). PCR genotyping of the colonies that survived in the IFN-treated *mDom*$^{\Delta/fl}$*;Mx1-Cre* BM culture revealed that the small number of surviving colonies arose from cells that escaped the induced deletion of the floxed mDom gene (data not shown). These results indicated that mDomino-deleted hematopoietic progenitors rapidly, and cell autonomously, lose the ability to proliferate.

mDomino Is Necessary for the Cell-cycle Progression of Embryonic Fibroblasts—The rapid proliferation arrest and/or apoptosis in mDom-deleted BM hematopoietic cells suggested that mDomino could be involved generally in the cell growth regulation. To examine this possibility, we prepared MEFs from *mDom*$^{fl/fl}$ mice and control *mDom*$^{fl/+}$ mice, and immortalized them by the 3T3 passage method. To inducibly inactivate the *mDom*^{fl} allele, the immortalized MEFs were infected with a recombinant retrovirus expressing Cre-ER^{T2} (hereafter simply CreER), which can be activated by treatment with OHT (32). In the CreER-expressing MEFs, the *mDom*^{fl} allele was deleted within a day after OHT treatment (Fig. 4*A*), and the mDomino protein disappeared concomitantly from the cell lysates (Fig. 4*B*). The OHT-induced deletion of mDomino resulted in the rapid and strong growth inhibition of *mDom*$^{fl/fl}$*; CreER* MEFs but not of the vector control *mDom*$^{fl/fl}$ MEFs (Fig. 4*C*). Another control cell line, *mDom*$^{+/fl}$*;CreER* MEF, which was established by the CreER-retrovirus infection of heterozygous *mDom*$^{fl/+}$ MEFs, grew normally even after the induced activation of CreER (Fig. 4*D*). These results indicated that the growth of MEFs is not affected by the addition of OHT or by the activation of the CreER protein and that mDomino is essential for their proliferation. In addition, microscopic examination revealed the emergence of a bi- or multi-nucleated population among the mDomino-deleted MEFs that had an enlarged cell body, abnormal nuclear morphology, and micronuclei (Fig. 4, *E* and *F*).

The above results suggested that mDomino plays an important role in cell-cycle regulation. We therefore analyzed the cell-cycle profiles of mDomino-deleted MEFs by flow cytometry. As shown in Fig. 5 (*A* and *B*), the *mDom*$^{fl/fl}$*;CreER* MEFs treated with OHT showed a significant increase in the population with 4N DNA content and the emergence of polyploid (>4N) cells. To examine the effect of the mDomino deficiency on cell-cycle progression, *mDom*$^{fl/fl}$*;CreER* MEFs were treated with OHT, driven into quiescence by serum starvation, and then released

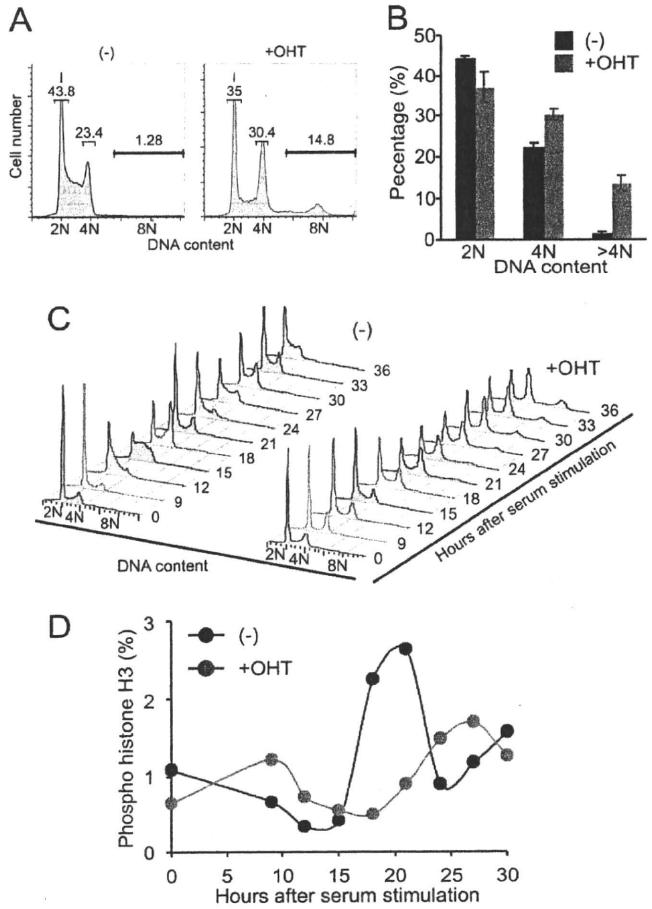

FIGURE 5. **mDomino-deficient MEFs exhibit polyploidy and defective cell-cycle progression.** *A*, the DNA content of OHT-treated or untreated (−) *mDom*$^{fl/fl}$*;CreER* MEFs was determined by flow cytometry after propidium iodide staining. *B*, the percentage of cells with 2N, 4N, and >4N DNA content in *A* was determined in three independent experiments. *C* and *D*, cell-cycle profile of *mDom*$^{fl/fl}$*;CreER* MEFs. Cells were treated with (+) or without (−) OHT for 8 h, serum-starved for 24 h, and then released from the starvation by stimulation with 10% fetal bovine serum. The cells were then collected at the indicated times and subjected to the flow cytometric analysis of their DNA content by propidium iodide staining (*C*), or of the mitotic index by staining with a phospho-Ser-10-specific, anti-histone H3 antibody (*D*).

back into the cell-cycle by the addition of serum. As shown in Fig. 5*C*, the mock-treated cells synchronously entered the S phase 12–15 h after serum stimulation, reached the G_2/M phase at about 18 h, and returned to the G_1 phase at 21 h. In contrast, MEFs treated with OHT displayed a small delay in entering the S phase and a slow but continuous increase in a population with 4N DNA content. This 4N population seemed to include not only the G_2/M population but also an aberrant cell population that had initiated a new round of DNA synthesis without cytokinesis (endoreduplication), which resulted in the accumulation of tetraploid cells with ~8N DNA content. To examine whether mDomino-deficient MEFs entered mitosis, MEFs re-stimulated with serum were stained with a phospho-Ser10-specific anti-histone H3 antibody, and quantified by flow cytometry (Fig. 5*D*). Mock-treated MEFs showed a sharp M-phase peak 18–20 h after stimulation, whereas the mDomino-deficient MEFs showed a delayed entry into mitosis. These results indicated that the depletion of mDomino causes the malfunction of the cell-cycle regulation at multiple steps, especially in the G_2/M phase, and eventually leads to the aberrant mitosis known as "mitotic catastrophe."

p400/mDomino was shown to participate in the adenovirus-E1A-induced transformation process through interaction with the N-terminal region of E1A (3). To examine whether expression of E1A affects the cell cycle defect caused by mDomino deletion, *mDom*$^{fl/fl}$*;CreER* MEFs were infected with retroviral constructs expressing wild-type 12 S E1A or *dl*1102(Δ26–35) mutant that was defective in interaction with mDomino. Resulting MEFs that overexpressed E1A or *dl*1102 grew faster than the parental MEFs or vector control cells, but were growth-arrested soon after the OHT treatment (supplemental Fig. 1), suggesting that overexpression of E1A protein cannot compensate for the mDomino deletion.

To confirm that the observed phenotypes of mDomino-deleted MEFs were caused by the absence of mDomino protein and not by other unexpected events, such as genomic recombination caused by CreER, *mDom*$^{fl/fl}$*;CreER* MEFs were transfected with an expression plasmid for HA-tagged mDomino (pNEF-DomHA), and stable cell lines were analyzed. As shown in Fig. 6, *mDom*$^{fl/fl}$*;CreER* cells expressing mDomino-HA displayed normal proliferation, cell-cycle distribution, and nuclear morphology irrespective of the OHT-induced deletion of the endogenous mDomino. This showed that the cell-cycle deficiency could be rescued by the exogenous expression of the wild-type mDomino protein and was, therefore, due to the absence of mDomino.

Impairment of Cell-cycle Regulatory Gene Expression in mDomino-deficient Cells—The p400/mDomino chromatin-remodeling complex is known to interact physically or functionally with cell-cycle-regulatory transcription factors, including c-Myc, E1A, p53, and E2F (3, 17–20). To gain insight into the molecular function of mDomino in cell-cycle regulation, we characterized the gene expression profiles of *mDom*$^{fl/fl}$*;CreER* MEFs treated or untreated with OHT by DNA microarray analysis (n = 3 for both untreated and OHT-treated cells), which revealed that 770 genes were differentially (≥2.0-fold) expressed by mDomino depletion, including 191 down-regulated genes (supplemental Table 1) and 579 up-regulated genes (data not shown). A gene annotation analysis revealed that, among the 93 genes whose expression was reduced to <45% by OHT treatment, many (27 genes) are characterized as cell-cycle-related genes, such as *E2F2*, *E2F7*, *E2F8*, *CENP-F* (*cenpf*), *Skp2*, *Nek2*, and *Cyclin A2* (*ccna2*) (Table 1). Moreover, 17 of the 93 genes are known Myc targets (supplemental Table 1) (Myc Cancer Gene, available on-line).

To confirm the microarray data and to characterize the time course of mRNA expression during cell-cycle progression, we carried out quantitative RT-PCR analysis of the genes for *Skp2*, *PLK1*, *CENP-F*, and *FoxM1*. As reported previously, the expressions of these genes were dependent on cell-cycle progression in the control *mDom*$^{fl/fl}$*;CreER* MEFs (Fig. 7*A*). In cells treated with OHT, the expression levels of these genes were low, and they were not clearly induced after the serum stimulation. We have also compared expression of *c-Myc*, *E2F1*, *p53*, and *H2A.Z* genes in the OHT-treated or -untreated cells. Expression levels of *p53* and *H2A.Z* in the mDomino-deleted cells were consis-

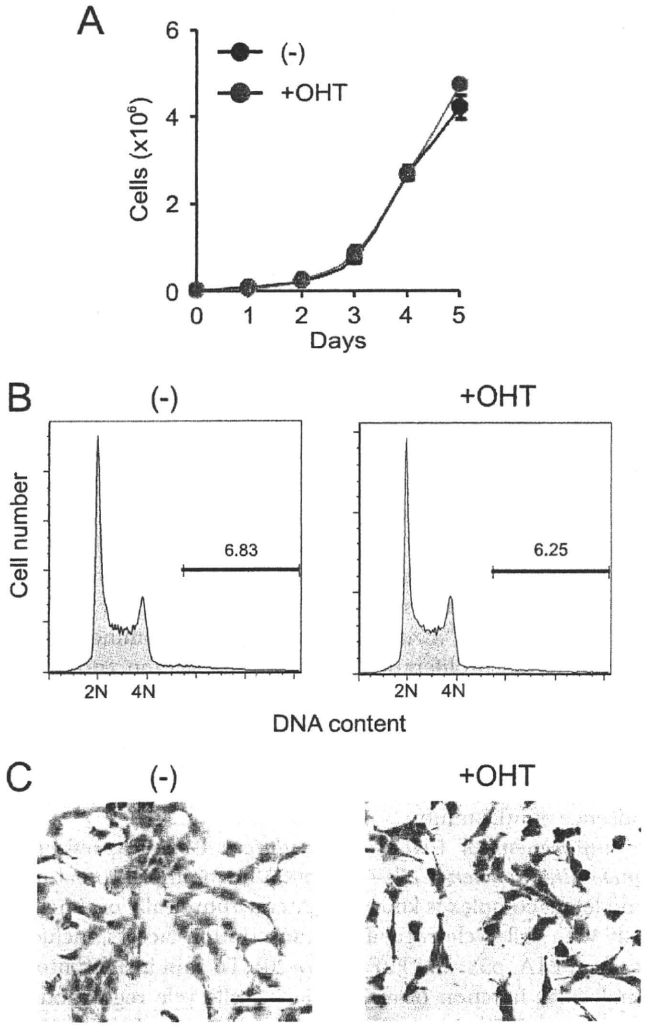

FIGURE 6. **Rescue of the cell-cycle phenotype by the exogenous expression of mDomino cDNA.** *mDom$^{fl/fl}$;CreER* MEFs were transfected with an mDomino expression plasmid, and stable transformants were cultured with or without OHT treatment. *A*, growth curve of the transformant MEFs treated with (+) or without (−) OHT. Data are the means ± S.D. of three separate experiments. *B*, cell-cycle profiles of the transformants treated without or with OHT and then cultured for 6 days. *C*, Wright-Giemsa staining of the transformants grown as in *B*. *Scale bars* represent 100 μm.

TABLE 1
Cell-cycle-related genes affected by mDomino deletion

DNA microarray analysis of OHT-treated (+OHT) or untreated (−) *mDom$^{fl/fl}$;CreER* MEFs were performed as described under "Experimental Procedures." Among the 93 genes whose expression was reduced to <45% by OHT treatment (supplemental Table 1), genes that are characterized as "cell cycle" are listed.

Gene symbol	-fold change	+OHT	(−)	*p* value	Accession number
E2f2	3.5	30	107	7.33E-05	BB543028
Mybl2	3.2	208	666	2.42E-04	NM_008652
Cenpf	3.2	97	310	1.02E-02	BB667318
Psrc1	3.0	288	878	4.66E-04	NM_019976
Fbxo5	3.0	618	1851	7.31E-05	AK011820
E2f7	2.7	557	1517	3.98E-03	BG069355
Cdc6	2.7	564	1531	4.25E-05	NM_011799
Ccna2	2.6	2615	6868	2.04E-03	X75483
Ccnf	2.6	144	378	3.59E-03	BB089717
Rbl1	2.6	178	465	2.64E-04	U27178
E2f8	2.6	336	876	2.80E-05	BM247465
Rcc1	2.6	470	1213	5.99E-06	NM_133878
2810433K01Rik	2.5	581	1461	2.32E-04	NM_025581
Mapk12	2.5	134	336	6.35E-04	BC021640
Cdca3	2.5	1732	4277	1.52E-03	BI081061
Uhrf1	2.4	192	470	6.75E-03	BB702754
Suv39h2	2.4	353	854	7.45E-04	NM_022724
Plk1	2.4	742	1787	3.42E-05	NM_011121
Rassf1	2.4	83	198	2.07E-03	BB385028
Cdc25a	2.4	590	1405	1.46E-02	C76119
Nek2	2.4	339	802	3.80E-04	NM_010892
Skp2	2.3	221	518	1.43E-02	AV259620
Sgol1	2.3	314	732	3.92E-03	BB410537
Incenp	2.3	87	201	2.06E-04	AV301185
Mcm3	2.3	234	531	1.02E-03	BI658327
Cdc20	2.2	2367	5311	3.80E-03	NM_023223
Ncapg2	2.2	1610	3593	1.26E-03	NM_133762

tently lower than those in the untreated cells. Unexpectedly, the expression of *c-Myc* and *E2F1* genes was rather up-regulated in the mDomino-deficient MEFs (Fig. 7*B*), suggesting that mDomino may be involved in repression of these genes by a direct mechanism or by an indirect, feedback pathway. RT-PCR analysis of the mDomino mRNA showed that the expression of mDomino in normal cells was independent of the cell cycle (supplemental Fig. 2). Finally, we examined whether the impaired expression of the cell-cycle-related genes could be rescued by the exogenous expression of mDomino protein. The *mDom$^{fl/fl}$;CreER* MEFs expressing mDomino-HA exhibited a normal expression of the cell-cycle-regulated genes irrespective of OHT treatment (Fig. 7*C*). In contrast, the expression of c-Myc, which was up-regulated in the mDom-deficient cells, was reduced to normal by the mDomino expression (Fig. 7*D*). Together, these results indicated that mDomino plays an essential role in the expression of various genes that are involved in cell-cycle regulation and suggested that the impaired expression of those genes causes the aberrant cell-cycle progression, growth arrest, and mitotic catastrophe of the mDomino-deficient cells.

DISCUSSION

In this report, we generated conditional knock-out mice of the p400/mDomino gene. These mice died within 2 weeks of pI:pC-induced, Mx1-Cre-mediated mDomino depletion. We showed that the mDomino deletion in BM cells resulted in the rapid loss of committed myeloid and erythroid cells as well as hematopoietic progenitor/stem cells. The extinction of hematopoietic cells from the BM was probably due to both a decrease in the proliferation and an increase in the apoptotic cell death of the mDomino-deleted cells, followed by their clearance and replacement by mature erythrocytes. A hematopoietic colony formation assay demonstrated that the IFN-induced deletion of mDomino strongly inhibited the growth of all the colony-forming progenitors, including the myeloid, erythroid, and megakaryocytic lineages, suggesting that the impaired hematopoiesis was cell autonomous and not caused by a defect in the hematopoiesis-supporting environment in the BM.

The strong growth inhibition of the mDomino-deficient hematopoietic cells prompted us to investigate the cell proliferation using embryonic fibroblasts from *mDom$^{fl/fl}$* mice. The induced deletion of the mDomino gene led to an acute and strong inhibition of the cellular proliferation of MEFs. Cell-cycle analysis revealed that the mDomino-deficient MEFs exhibited pleiotropic cell-cycle defects, including delayed and insufficient entry into the S phase, increase in the G_2/M phase,

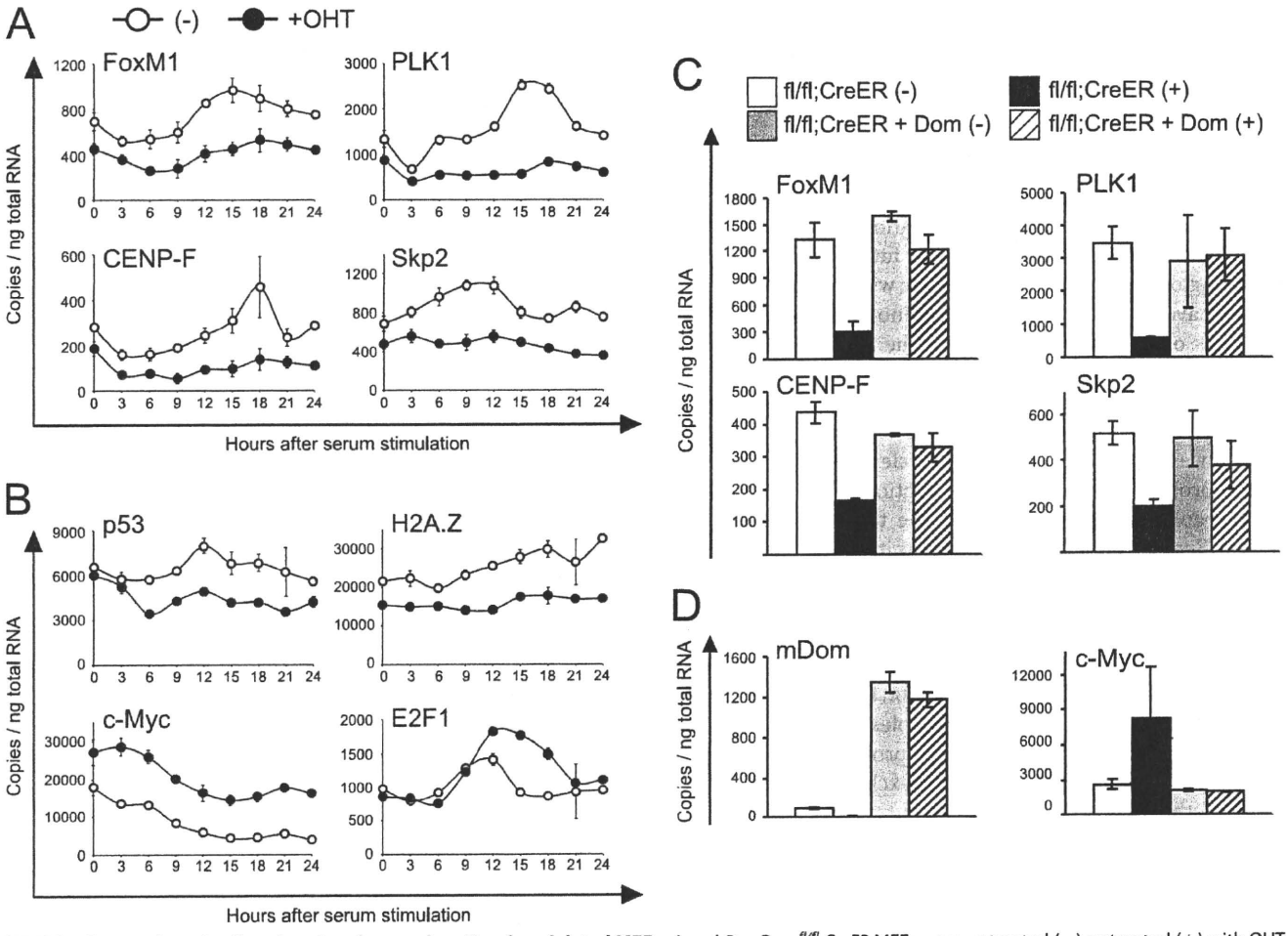

FIGURE 7. **Expression of cell-cycle-related genes in mDomino-deleted MEFs.** *A* and *B*, *mDom$^{fl/fl}$;CreER* MEFs were untreated (−) or treated (+) with OHT, serum-starved for 24 h, and then re-stimulated with 10% fetal bovine serum. At the indicated times, the RNA was extracted and analyzed for expression of the indicated genes by quantitative RT-PCR. *C* and *D*, parental *mDom$^{fl/fl}$;CreER* MEFs and mDomino-expressing transformants (*fl/fl;CreER + Dom*) were untreated (−) or treated (+) with OHT, cultured for 3 days, and then subjected to expression analysis by quantitative RT-PCR.

and the accumulation of polyploid and/or multinucleated cells with micronuclei. These phenotypes are very similar to those of *Trrap*-deleted MEFs, in which a spindle checkpoint failure leads to mitotic catastrophe (33), suggesting that the polyploid and/or multinucleated population of mDom-deficient cells might arise from a failure in mitotic checkpoint followed by endoreduplication of the DNA without cytokinesis. In *Saccharomyces cerevisiae*, the Swr1 complex is involved in chromosome segregation and plays an important role in chromosome stability (34). In addition, the TRRAP-Tip60 complex, which also contains p400/mDomino, is known to be required for the recruitment and accumulation of DNA repair proteins at sites of DNA double-strand break (35). Thus, p400/mDomino may also be involved in maintaining chromosome integrity.

In the human osteosarcoma U2OS cell line and primary fibroblasts, the shRNA-mediated knockdown of p400/mDomino results in the induction of cell-cycle inhibitor p21, cell-cycle arrest at G_1, and premature senescence (21, 22). However, the mDomino-deleted MEFs, which also showed strong growth inhibition, did not show up-regulated *p21* expression (data not shown), suggesting that the loss of mDomino can block the cell cycle by a mechanism other than the p53-p21 pathway. Our DNA microarray analysis showed that the expression levels of many cell-cycle-related genes were significantly reduced in the mDomino-deleted MEFs. Interestingly, among the strongly affected genes, *CENP-F*, *Nek2*, and *Plk1* are representative G_2/M-specific genes that are regulated by the transcription factor FoxM1 (36–38), which was also among the strongly reduced genes. This finding indicates that the cell-cycle phenotypes of the mDomino-deficient MEFs were at least partly due to the impaired expression of FoxM1 and its target genes. In this regard, it is noteworthy that *FoxM1*-deficient MEFs exhibit mitotic malfunction similar to our results (36). However, the exogenous overexpression of FoxM1 cDNA in *mDom$^{fl/fl}$;CreER* MEFs failed to rescue the cell-cycle phenotype (data not shown), suggesting that p400/mDomino is responsible for the regulated expression not only of FoxM1 targets but also of other cell-cycle-related genes. A candidate transcription factor of note is the oncoprotein c-Myc, which interacts with the Tip60-TRRAP-p400/mDomino complex and regulates the expression of various genes positively or negatively, possibly through the histone-acetyl-transferring and/or the H2A.Z-exchanging activities of the complex (3, 17, 19). This hypothesis is consistent with the results of our microarray analysis

(supplemental Table 1), in which the strongly affected genes included several Myc targets, such as *E2F2*, *Mybl2*, *Cdc6*, *Cyclin A*, and *FoxM1* (39–43). To elucidate whether p400/mDomino is directly involved in the regulatory expression of these genes, we need to investigate physical and functional interactions of the p400/mDomino chromatin-remodeling complex with the c-Myc and/or FoxM1 on the promoter region of their target genes by chromatin immunoprecipitation analyses using cell-cycle-synchronized fibroblasts, in our future experiments.

Taking our present results together with our previous studies, we have shown that p400/mDomino is essential for hematopoiesis of both the yolk sac and the adult BM. The acute extinction of hematopoietic cells is probably due to the strong growth inhibition and apoptotic cell death of the mDomino-deleted cells. We also provide evidence that p400/mDomino plays an essential role in the cell-cycle progression of fibroblasts, probably through its transcriptional activation of cell-cycle-regulatory genes, especially the targets of FoxM1 and c-Myc. Because p400/mDomino exerts its chromatin-remodeling function via its H2A.Z-exchange activity, the interaction of p400/mDomino with c-Myc (and possibly with FoxM1) might regulate the deposition and/or eviction of the H2A.Z variant at the promoter nucleosome of cell-cycle-regulatory genes (14, 16, 44). Future studies on the interaction between transcription factors and the p400/mDomino complex and their role in the H2A.Z-positioning mechanism will provide insight into the biological significance of the H2A.Z-exchanging machinery in cell growth and differentiation.

Acknowledgments—We are grateful to Dr. Shigeyoshi Itohara and the RIKEN BioResource Center for providing the FLPe transgenic mice. We also thank Dr. Toru Nakano for the Cre-ER^{T2} construct, and Dr. Joe S. Mymryk for the E1A cDNAs.

REFERENCES

1. Saha, A., Wittmeyer, J., and Cairns, B. R. (2006) *Nat. Rev. Mol. Cell Biol.* **7,** 437–447
2. Cairns, B. R. (2007) *Nat. Struct. Mol. Biol.* **14,** 989–996
3. Fuchs, M., Gerber, J., Drapkin, R., Sif, S., Ikura, T., Ogryzko, V., Lane, W. S., Nakatani, Y., and Livingston, D. M. (2001) *Cell* **106,** 297–307
4. Ogawa, H., Ueda, T., Aoyama, T., Aronheim, A., Nagata, S., and Fukunaga, R. (2003) *Genes Cells* **8,** 325–339
5. Kobor, M. S., Venkatasubrahmanyam, S., Meneghini, M. D., Gin, J. W., Jennings, J. L., Link, A. J., Madhani, H. D., and Rine, J. (2004) *PLoS Biol.* **2,** E131
6. Ruhf, M. L., Braun, A., Papoulas, O., Tamkun, J. W., Randsholt, N., and Meister, M. (2001) *Development* **128,** 1429–1441
7. Cai, Y., Jin, J., Florens, L., Swanson, S. K., Kusch, T., Li, B., Workman, J. L., Washburn, M. P., Conaway, R. C., and Conaway, J. W. (2005) *J. Biol. Chem.* **280,** 13665–13670
8. Jin, J., Cai, Y., Yao, T., Gottschalk, A. J., Florens, L., Swanson, S. K., Gutiérrez, J. L., Coleman, M. K., Workman, J. L., Mushegian, A., Washburn, M. P., Conaway, R. C., and Conaway, J. W. (2005) *J. Biol. Chem.* **280,** 41207–41212
9. Krogan, N. J., Keogh, M. C., Datta, N., Sawa, C., Ryan, O. W., Ding, H., Haw, R. A., Pootoolal, J., Tong, A., Canadien, V., Richards, D. P., Wu, X., Emili, A., Hughes, T. R., Buratowski, S., and Greenblatt, J. F. (2003) *Mol. Cell* **12,** 1565–1576
10. Mizuguchi, G., Shen, X., Landry, J., Wu, W. H., Sen, S., and Wu, C. (2004) *Science* **303,** 343–348
11. Kusch, T., Florens, L., Macdonald, W. H., Swanson, S. K., Glaser, R. L., Yates, J. R., 3rd, Abmayr, S. M., Washburn, M. P., and Workman, J. L. (2004) *Science* **306,** 2084–2087
12. Jin, J., Cai, Y., Li, B., Conaway, R. C., Workman, J. L., Conaway, J. W., and Kusch, T. (2005) *Trends Biochem. Sci.* **30,** 680–687
13. van Attikum, H., and Gasser, S. M. (2005) *Nat. Rev. Mol. Cell Biol.* **6,** 757–765
14. Squatrito, M., Gorrini, C., and Amati, B. (2006) *Trends Cell Biol.* **16,** 433–442
15. Morrison, A. J., and Shen, X. (2009) *Nat. Rev. Mol. Cell Biol.* **10,** 373–384
16. Svotelis, A., Gévry, N., and Gaudreau, L. (2009) *Biochem. Cell Biol.* **87,** 179–188
17. Frank, S. R., Parisi, T., Taubert, S., Fernandez, P., Fuchs, M., Chan, H. M., Livingston, D. M., and Amati, B. (2003) *EMBO Rep.* **4,** 575–580
18. Taubert, S., Gorrini, C., Frank, S. R., Parisi, T., Fuchs, M., Chan, H. M., Livingston, D. M., and Amati, B. (2004) *Mol. Cell. Biol.* **24,** 4546–4556
19. Gévry, N., Chan, H. M., Laflamme, L., Livingston, D. M., and Gaudreau, L. (2007) *Genes Dev.* **21,** 1869–1881
20. Lu, J., Ruhf, M. L., Perrimon, N., and Leder, P. (2007) *Proc. Natl. Acad. Sci. U.S.A.* **104,** 9381–9386
21. Chan, H. M., Narita, M., Lowe, S. W., and Livingston, D. M. (2005) *Genes Dev.* **19,** 196–201
22. Tyteca, S., Vandromme, M., Legube, G., Chevillard-Briet, M., and Trouche, D. (2006) *EMBO J.* **25,** 1680–1689
23. Fazzio, T. G., Huff, J. T., and Panning, B. (2008) *Cell* **134,** 162–174
24. Ueda, T., Watanabe-Fukunaga, R., Ogawa, H., Fukuyama, H., Higashi, Y., Nagata, S., and Fukunaga, R. (2007) *Genes Cells* **12,** 581–592
25. Kanki, H., Suzuki, H., and Itohara, S. (2006) *Exp. Anim.* **55,** 137–141
26. Williams-Simons, L., and Westphal, H. (1999) *Transgenic Res.* **8,** 53–54
27. Kühn, R., Schwenk, F., Aguet, M., and Rajewsky, K. (1995) *Science* **269,** 1427–1429
28. Ueda, T., Watanabe-Fukunaga, R., Fukuyama, H., Nagata, S., and Fukunaga, R. (2004) *Mol. Cell. Biol.* **24,** 6539–6549
29. Weischenfeldt, J., Damgaard, I., Bryder, D., Theilgaard-Mönch, K., Thoren, L. A., Nielsen, F. C., Jacobsen, S. E., Nerlov, C., and Porse, B. T. (2008) *Genes Dev.* **22,** 1381–1396
30. Morita, S., Kojima, T., and Kitamura, T. (2000) *Gene Ther.* **7,** 1063–1066
31. Iida, S., Kohro, T., Kodama, T., Nagata, S., and Fukunaga, R. (2005) *J. Leukoc. Biol.* **78,** 481–490
32. Feil, R., Wagner, J., Metzger, D., and Chambon, P. (1997) *Biochem. Biophys. Res. Commun.* **237,** 752–757
33. Herceg, Z., Hulla, W., Gell, D., Cuenin, C., Lleonart, M., Jackson, S., and Wang, Z. Q. (2001) *Nat. Genet.* **29,** 206–211
34. Krogan, N. J., Baetz, K., Keogh, M. C., Datta, N., Sawa, C., Kwok, T. C., Thompson, N. J., Davey, M. G., Pootoolal, J., Hughes, T. R., Emili, A., Buratowski, S., Hieter, P., and Greenblatt, J. F. (2004) *Proc. Natl. Acad. Sci. U.S.A.* **101,** 13513–13518
35. Murr, R., Loizou, J. I., Yang, Y. G., Cuenin, C., Li, H., Wang, Z. Q., and Herceg, Z. (2006) *Nat. Cell Biol.* **8,** 91–99
36. Laoukili, J., Kooistra, M. R., Brás, A., Kauw, J., Kerkhoven, R. M., Morrison, A., Clevers, H., and Medema, R. H. (2005) *Nat. Cell Biol.* **7,** 126–136
37. Laoukili, J., Stahl, M., and Medema, R. H. (2007) *Biochim. Biophys. Acta* **1775,** 92–102
38. Fu, Z., Malureanu, L., Huang, J., Wang, W., Li, H., van Deursen, J. M., Tindal, D. J., and Chen, J. (2008) *Nat. Cell Biol.* **10,** 1076–1082
39. Menssen, A., and Hermeking, H. (2002) *Proc. Natl. Acad. Sci. U.S.A.* **99,** 6274–6279
40. Fernandez, P. C., Frank, S. R., Wang, L., Schroeder, M., Liu, S., Greene, J., Cocito, A., and Amati, B. (2003) *Genes Dev.* **17,** 1115–1129
41. Li, Z., Van Calcar, S., Qu, C., Cavenee, W. K., Zhang, M. Q., and Ren, B. (2003) *Proc. Natl. Acad. Sci. U.S.A.* **100,** 8164–8169
42. Menssen, A., Epanchintsev, A., Lodygin, D., Rezaei, N., Jung, P., Verdoodt, B., Diebold, J., and Hermeking, H. (2007) *Cell Cycle* **6,** 339–352
43. Herold, S., Herkert, B., and Eilers, M. (2009) *Nat. Rev. Cancer* **9,** 441–444
44. Martinato, F., Cesaroni, M., Amati, B., and Guccione, E. (2008) *PLoS One* **3,** e3650

Cell Death and Differentiation (2009), 1–11

www.nature.com/cdd

Apaf-1-independent programmed cell death in mouse development

A Nagasaka[1,2,5], K Kawane[1,3], H Yoshida[4] and S Nagata*[,1,2,3]

Many cells die during mammalian development and are engulfed by macrophages. In *DNase II*$^{-/-}$ embryos, the TUNEL-positive DNA of apoptotic cells is left undigested in macrophages, providing a system for studying programmed cell death during mouse development. Here, we showed that an *Apaf-1*-null mutation in the *DNase II*$^{-/-}$ embryos greatly reduced the number of macrophages carrying DNA at E11.5. However, at later stages of the embryogenesis, a significant number of macrophages carrying undigested DNA were present in *Apaf-1*$^{-/-}$ embryos, indicating that cells died and were engulfed in an *Apaf-1*-independent manner. In most tissues of the *Apaf-1*$^{-/-}$ embryos, no processed caspase-3 was detected, and the DNA of dead cells accumulated in the macrophages appeared intact. Many nonapoptotic dead cells were found in the tail of the *Apaf-1*$^{-/-}$ embryos, suggesting that the *Apaf-1*-independent programmed cell death occurred, and these dead cells were engulfed by macrophages. In contrast, active caspase-3 was detected in E14.5 thymus of *Apaf-1*$^{-/-}$ embryos. Treatment of fetal thymocytes with staurosporine, but not etoposide, induced processing of procaspases 3 and 9, indicating that the E14.5 thymocytes have the ability to undergo caspase-dependent apoptosis in an *Apaf-1*-independent manner. Thus, programmed cell death in mouse development, which normally proceeds in an efficient Apaf-1-depenent mechanism, appears to be backed up by Apaf-1-independent death systems.
Cell Death and Differentiation advance online publication, 4 December 2009; doi:10.1038/cdd.2009.186

Many useless and toxic cells are generated during animal development and removed by programmed cell death, which is mainly mediated by apoptosis.[1,2] Apoptosis is accompanied by morphological changes, such as the blebbing and condensation of cells, loss of membrane symmetry, and nuclear condensation.[3] Late in apoptosis, dying cells are fragmented into small 'apoptotic bodies,' which are recognized by phagocytes for engulfment. This morphological change in the cells and their rapid disposal are distinct from necrosis, in which cells swell, the plasma membranes are ruptured, and the cellular contents are believed to be released.

The signal transduction involved in apoptotic cell death has been intensively studied[4,5] and shown to proceed by two major pathways, an extrinsic and an intrinsic one. In the extrinsic pathway, signals from death receptors, such as Fas and TNF receptor, activate an initiator caspase, caspase-8, that activates downstream effector caspases, mainly caspase-3, leading to the cleavage of more than 300 cellular proteins.[6,7] One of the caspase-3 substrates is the inhibitor of caspase-activated DNase (CAD), and its cleavage by caspase-3 inactivates the ability to associate with CAD, allowing CAD to cause the fragmentation of chromosomal DNA into nucleosomal units.[8] In the intrinsic pathway, death signals cause the release of cytochrome *c* from mitochondria through 'BH3-only' proteins of the Bcl-2 family.[9,10] The cytochrome *c* binds to Apaf-1 and activates caspase-9, which leads to the activation of caspase-3 and CAD, resulting in the cleavage of cellular substrates and the fragmentation of chromosomal DNA. Apoptotic cells that die by either the intrinsic or the extrinsic pathway expose phosphatidylserine on their surface.[11] Macrophages and immature dendritic cells recognize the phosphatidylserine and rapidly engulf the apoptotic cells.[12] The engulfed dead cells are transferred to lysosomes, where all their components are degraded.

The role of the intrinsic apoptotic pathway in programmed cell death has been studied by establishing mice that lack genes involved in apoptotic signal transduction.[13–17] The results obtained with these knockout mice have not always been consistent among groups. For example, Yoshida *et al.*[14] and Kuida *et al.*[13] reported that Apaf-1 and caspase-9 are indispensable for the cell death induced by cytotoxic agents or γ-radiation in various tissues, whereas Marsden *et al.*[18] reported that lymphocytes undergo apoptosis without Apaf-1 or caspase-9 on cytokine deprivation. Furthermore, except for craniofacial abnormalities and the hyperproliferation of neuronal cells, *Apaf-1*-deficient mice are apparently normal, especially in the C57BL/6 background,[19] suggesting the presence of a back-up system for the Apaf-1-mediated apoptosis in mouse development.

[1]Department of Medical Chemistry, Graduate School of Medicine, Kyoto University, Yoshida-Konoe, Sakyo-ku, Kyoto 606-8501, Japan; [2]Department of Integrated Biology, Graduate School of Frontier Biosciences, Osaka University, 2-2 Yamada-oka, Suita, Osaka 565-0871, Japan; [3]Core Research for Evolutional Science and Technology, Japan Science and Technology Corporation, Yoshida-Konoe, Kyoto 606-8501, Japan and [4]Division of Molecular and Cellular Immunoscience, Department of Biomolecular Sciences, Faculty of Medicine, Saga University, 5-1-1 Nabeshima, Saga 849-8501, Japan
*Corresponding author: S Nagata, Department of Medical Chemistry, Graduate School of Medicine, Kyoto University, Yoshida-Konoe, Sakyo-ku, Kyoto 606-8501, Japan. Tel: +81 75 753 9441; Fax: +81 75 753 9446; E-mail: snagata@mfour.med.kyoto-u.ac.jp
[5]Current address: Tomita Pharmaceutical Co., Akinokami, Seto-cho, Tokushima 771-0306, Japan.
Keywords: apoptosis; caspase; DNase II; macrophage; necrosis; TUNEL
Abbreviations: CAD, caspase-activated DNase; mAb, monoclonal antibody
Received 01.10.09; revised 29.10.09; accepted 04.11.09; Edited by G Melino

Because dying cells are swiftly engulfed and degraded by macrophages, the detection of apoptotic cells in animals is not an easy task. DNase II is responsible for digesting the DNA of apoptotic cells after macrophages engulf them, and many macrophages carrying engulfed DNA are present in *DNase II*-deficient embryos.[20–22] Here, we used *DNase II*-deficient mice to detect the programmed cell death that occurs during mouse development, and found that Apaf-1 seems to be dispensable for this process. In the thymus of *Apaf-1*$^{-/-}$ embryos at E14.5, caspases were activated in an Apaf-1-independent manner. In most other tissues, cells died by an Apaf-1-independent nonapoptotic mechanism, and were engulfed by macrophages. These results indicate that Apaf-1-independent systems, with or without caspase activation, function as back-up systems for the programmed cell death in mammalian development.

Results

Apaf-1-dependent programmed cell death in mouse embryos at E11.5. When we used the TUNEL staining to detect apoptotic cells in E11.5 wild-type mouse embryos, it yielded barely detectable signals (data not shown). A mutation of *nuc-1*, a homologue of *DNase II*, enhances the TUNEL positivity in *C. elegans*.[23] Similarly, the mouse *DNase II*$^{-/-}$ embryos showed very strong TUNEL signals (Figure 1a), which is due to the accumulation of DNA fragmented by CAD.[24] TUNEL-positive spots were frequent in several regions, such as the diencephalon at the cerebrum, the lamina terminalis, somites, and mesonephric ducts. Observations at higher magnification showed TUNEL positivity in these regions was much stronger in the *DNase II*$^{-/-}$ than the wild-type embryos. The TUNEL-positive spots in the *DNase II*$^{-/-}$ embryos were clustered into foci that were strongly DAPI positive (Figure 1b). The foci were located inside F4/80-positive macrophages, suggesting that they were the DNA of engulfed apoptotic cells. The engulfment of corpses in *C. elegans* requires the activation of caspase; a mutation in *Ced-3* or *Ced-4*, homologues of caspase and Apaf-1, respectively, prevents the engulfment of cell corpses.[25] Accordingly, a null mutation of *Apaf-1* blocked the generation of TUNEL-positive foci (Figure 1a and b), indicating that the apoptotic cell death and engulfment of dead cells in the E11.5 mouse embryos were apparently Apaf-1 dependent.

Apaf-1-independent programmed cell death in mouse embryos. Many TUNEL-positive foci were observed throughout the *DNase II*$^{-/-}$ embryos at E14.5 as well (data not shown). *DNase II*$^{-/-}$ embryos produce IFNβ which is lethal, but the lethality can be rescued by a deficiency of IFN type I receptor.[26] To exclude the possible cell death caused by IFNβ, we carried out the TUNEL staining with *DNase II*$^{-/-}$ *IFN-IR*$^{-/-}$ embryos. Many TUNEL-positive foci still could be detected in various tissues of *DNase II*$^{-/-}$*IFN-IR*$^{-/-}$ embryos (Figure 2a ; data not shown), suggesting that the death of the cells in *DNase II*$^{-/-}$ embryos was intrinsic to mouse embryogenesis, and not due to the secondary effect by IFNβ. The null mutation of *Apaf-1* blocked the generation of TUNEL-positive foci in most tissues of the E14.5 *DNase II*$^{-/-}$*IFN-IR*$^{-/-}$ embryos. For example, many TUNEL-positive foci were present at the interdigits of the hind paw of *DNase II*$^{-/-}$*IFN-IR*$^{-/-}$ embryos, and activated caspase-3 could be detected in this region (Figure 2a and b). The deficiency of *Apaf-1* prevented both the caspase activation and the appearance of TUNEL-positive foci. Probably due to the inhibition of apoptotic cell death, the formation of interdigits was retarded in the *Apaf-1*$^{-/-}$*DNase II*$^{-/-}$*IFN-IR*$^{-/-}$ embryos compared with *Apaf-1*$^{+/+}$*DNase II*$^{-/-}$*IFN-IR*$^{-/-}$ embryos, as reported for *Apaf-1*-null mice.[14]

At E17.5, fewer DAPI-positive foci were detected in the *Apaf-1*$^{+/+}$*DNase II*$^{-/-}$*IFN-IR*$^{-/-}$ embryos than at E14.5, as seen, for example, in the interdigits (Figure 2c), which have completely formed by E17.5. In contrast, the interdigits of the *Apaf-1*$^{-/-}$*DNase II*$^{-/-}$*IFN-IR*$^{-/-}$ embryos carried more DAPI-positive foci at E17.5 than at E14.5, and these DAPI-positive materials were located within F4/80-positive macrophages (Figure 2d). Electron microscopy showed that the DNA accumulated in the macrophages at the interdigits of the E17.5 *Apaf-1*$^{+/+}$*DNase II*$^{-/-}$*IFN-IR*$^{-/-}$ embryos is fragmented, whereas the DNA in the *Apaf-1*$^{-/-}$*DNase II*$^{-/-}$*IFN-IR*$^{-/-}$ embryos was apparently intact (Figure 2e). The active caspase-3 could be detected in the interdigits of *Apaf-1*$^{+/+}$ but not *Apaf-1*$^{-/-}$ embryos (data not shown). These results suggested that in late embryogenesis, the cells in the interdigits could die in an Apaf-1-independent manner, and the dead cells were engulfed by macrophages.

Apaf-1-independent nonapoptotic cell death. At the ventral ectodermal ridge of the tail in mouse embryos, many cells undergo programmed cell death, which was detected as DAPI-positive foci in the *DNase II*$^{-/-}$*IFN-IR*$^{-/-}$ embryos at E14.5 (Figure 3a and b). In the *Apaf-1*$^{+/+}$ embryos, the DNA that accumulated in the ridge was TUNEL positive, and many processed caspase-3-positive cells could be detected in this region. On the other hand, the DNA that accumulated in the *Apaf-1*$^{-/-}$ embryos was TUNEL negative, and processed caspase-3-positive cells were hardly detectable. Because the DAPI-positive foci were relatively closely clustered in the ventral ectodermal ridge of the tail (Figure 3c), we analyzed this region by electron microscopy. As shown in Figure 3d, many unengulfed, nonapoptotic dying cells were detected in the E14.5 *Apaf-1*$^{-/-}$ embryos. That is, the unengulfed dying cells showed mottled

Figure 1 Apaf-1-dependent programmed cell death in *DNase II*$^{-/-}$ mouse embryos at E11.5. (**a**) TUNEL staining of the E11.5 whole embryos. Paraffin sections from E11.5 *Apaf-1*$^{+/-}$*DNase II*$^{-/-}$ and *Apaf-1*$^{-/-}$*DNase II*$^{-/-}$ embryos were stained with TUNEL, followed by counterstaining with methyl green. Scale bar = 500 μm. (**b**) TUNEL staining of various tissues from E11.5 embryos. Paraffin sections of the diencephalon, lamina terminalis, and somites from E11.5 *Apaf-1*$^{+/-}$*DNase II*$^{+/+}$, *Apaf-1*$^{+/-}$*DNase II*$^{-/-}$, and *Apaf-1*$^{-/-}$*DNase II*$^{-/-}$ embryos, were stained with TUNEL, counterstained with methyl green, and observed by microscopy. For staining of F4/80, cryosections from E11.5 *Apaf-1*$^{+/-}$*DNase II*$^{-/-}$ mouse embryos were stained with DAPI and a rat mAb against mouse F4/80, followed by incubation with peroxidase-conjugated rabbit anti-rat Ig, and detected by Cy3-labeled tyramide. Staining profiles with DAPI and anti-F4/80 are merged, and shown in the middle panels. Polarity of the embryos is indicated in left panels. a, anterior; p, posterior; d, dorsal; v, ventral. Yellow arrowheads indicate the macrophages carrying undigested DNA. Scale bar = 100 μm

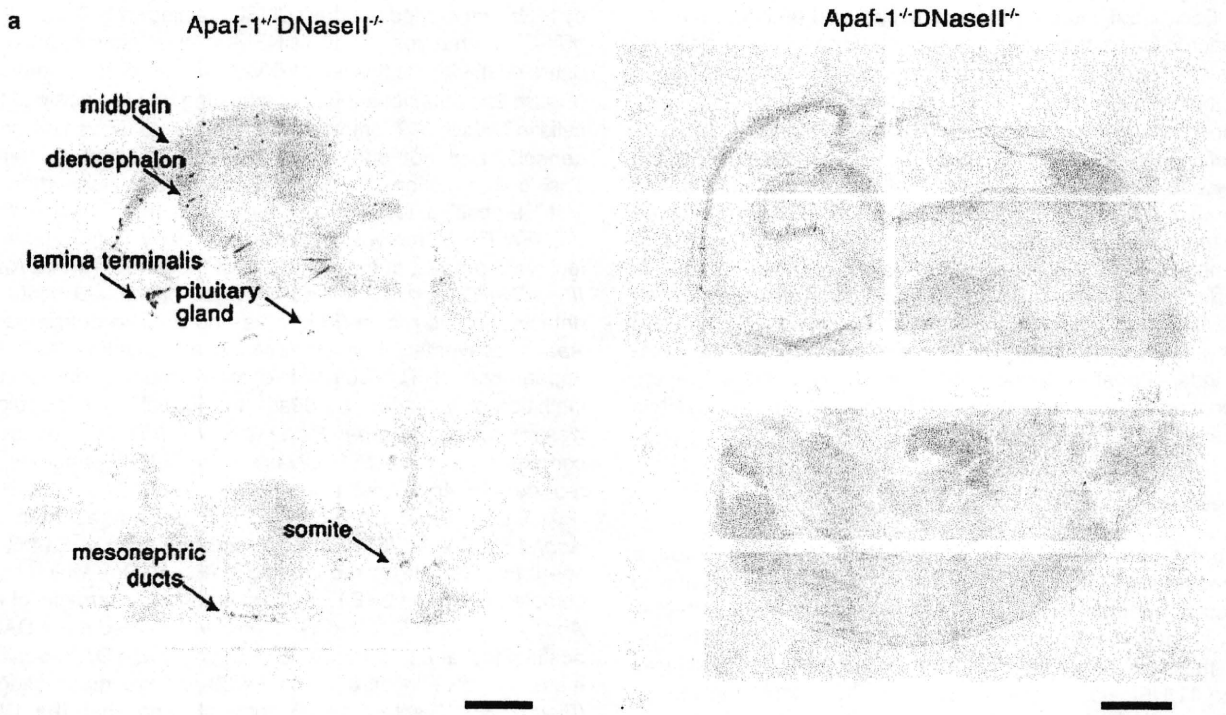
a
Apaf-1+/-DNaseII-/-
Apaf-1-/-DNaseII-/-
midbrain
diencephalon
lamina terminalis
pituitary gland
somite
mesonephric ducts

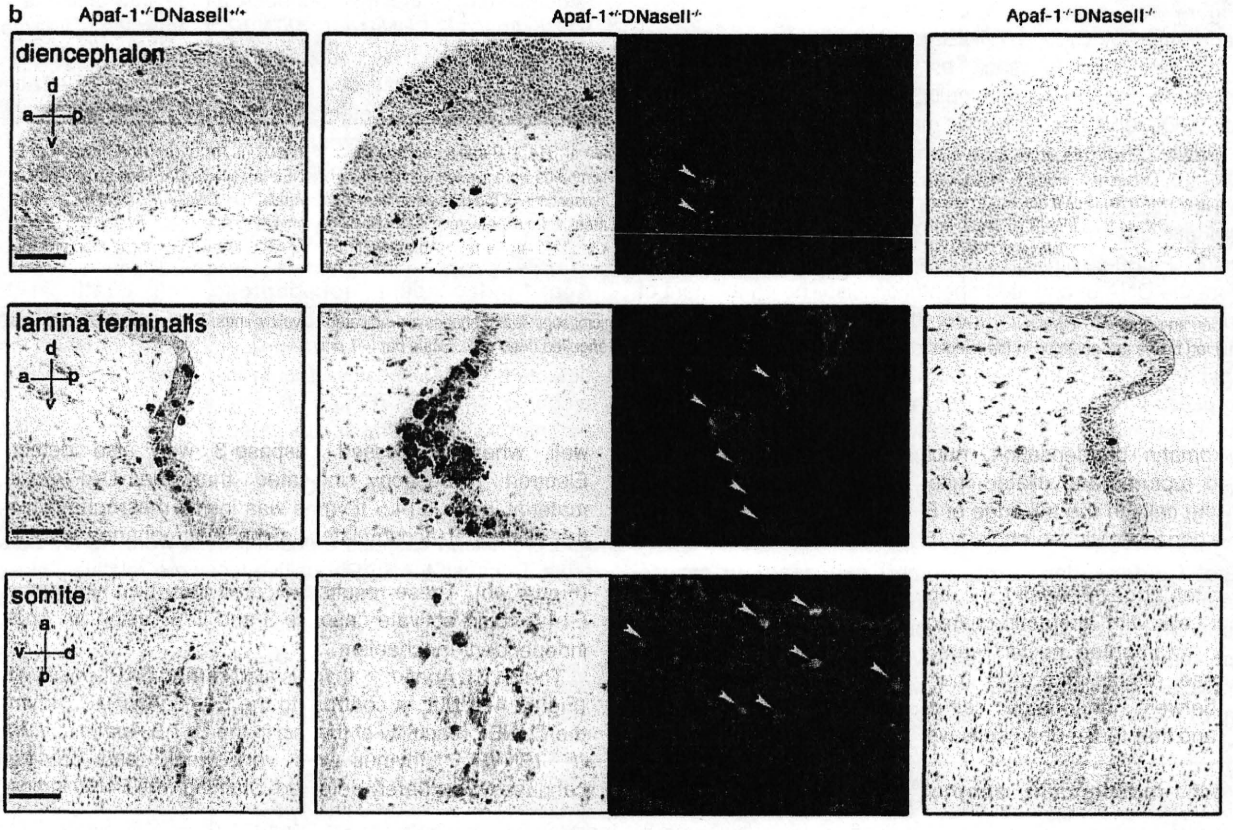
b
Apaf-1+/-DNaseII+/+
Apaf-1+/-DNaseII-/-
Apaf-1-/-DNaseII-/-
diencephalon
lamina terminalis
somite
d
a
p
v

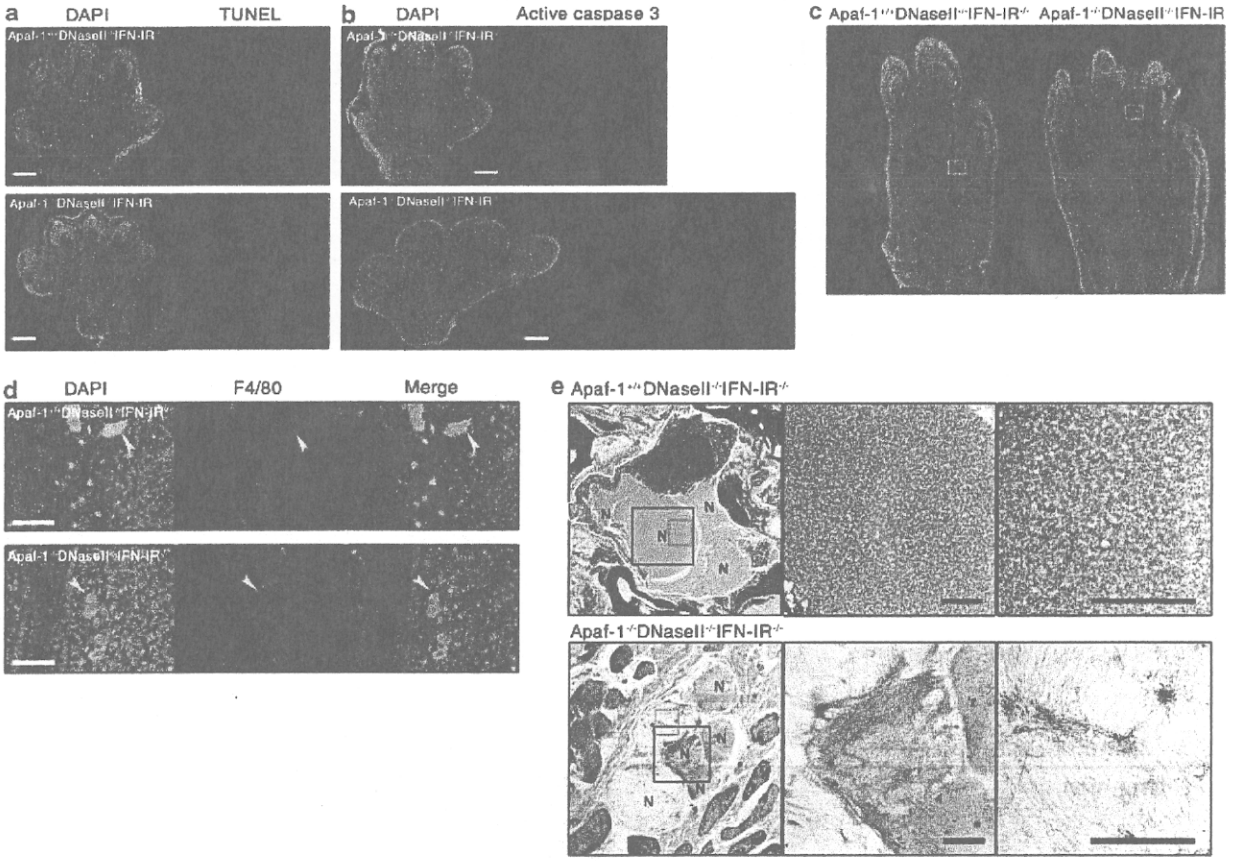

Figure 2 Programmed cell death in the interdigit. (**a** and **b**) Programmed cell death at E14.5. Paraffin sections (**a**) or cryosections (**b**) of the hind paws from E14.5 *Apaf-1*$^{+/+}$ *DNase II*$^{-/-}$ *IFN-IR*$^{-/-}$ (upper) and *Apaf-1*$^{-/-}$ *DNase II*$^{-/-}$ *IFN-IR*$^{-/-}$ (lower) embryos were stained with DAPI and TUNEL (**a**), or with DAPI and an anti-processed caspase-3 mAb (**b**). Scale bar = 100 μm. (**c** and **d**) Programmed cell death at E17.5. Cryosections of the hind paws from E17.5 *Apaf-1*$^{+/+}$ *DNase II*$^{-/-}$ *IFN-IR*$^{-/-}$ (left) and *Apaf-1*$^{-/-}$ *DNase II*$^{-/-}$ *IFN-IR*$^{-/-}$ (right) embryos were stained with DAPI (**c**). The boxed areas in (**c**) are enlarged in (**d**). Sections from E17.5 *Apaf-1*$^{+/+}$ *DNase II*$^{-/-}$ *IFN-IR*$^{-/-}$ (upper) and *Apaf-1*$^{-/-}$ *DNase II*$^{-/-}$ *IFN-IR*$^{-/-}$ (lower) mouse embryos were stained with DAPI and a rat mAb against mouse F4/80, followed by incubation with peroxidase-conjugated rabbit anti-rat Ig, and detected by Cy3-labeled tyramide. The staining profiles with DAPI and anti-F4/80 are merged in the right panels. Arrowheads indicate macrophages carrying engulfed DNA. Scale bars = 50 μm (**d**). (**e**) Electron microscopy. Sections from the E17.5 hind paws of *Apaf-1*$^{+/+}$ *DNase II*$^{-/-}$ *IFN-IR*$^{-/-}$ (upper) and *Apaf-1*$^{-/-}$ *DNase II*$^{-/-}$ *IFN-IR*$^{-/-}$ (lower) mice were analyzed by electron microscopy. Macrophages are indicated by yellow lines. The areas surrounded by black and red boxes are enlarged in the middle and right panels. N, nuclear DNA from the engulfed dead cells. Scale bar = 1 μm

chromatin condensation, nuclear membrane detachment and rupture, and dilated mitochondria. Approximately 5% of the cells in the tail ridge of E14.5 *Apaf-1*$^{-/-}$ embryos had the nonapoptotic morphology (Figure 3e), but apoptotic dying cells were hardly detectable. Nonapoptotic dead cells in the tail ridge of *Apaf-1*$^{+/+}$ embryos were rare, about 1%, but cells with apoptotic characteristics, such as condensed and fragmented nuclei, were relatively abundant (1.72%). These results indicated that the cells in the tail ridge underwent nonapoptotic cell death in the absence of Apaf-1, and that these dead cells were engulfed by macrophages.

Apaf-1-independent apoptosis in the thymus. Many TUNEL- and DAPI-positive foci were observed in the thymus of *DNase II*$^{-/-}$ *IFN-IR*$^{-/-}$ embryos at E14.5 (Figure 4a). In contrast to most other tissues, such as the interdigits and tails at this stage of embryogenesis, the TUNEL-positive foci were present in the *Apaf-1*$^{-/-}$ thymus as well, where processed caspase-3 was also detected. Electron microscopy indicated that the DAPI-positive material in the E14.5 thymus was inside macrophages, and the DNA that accumulated in the macrophages was fragmented in both the *Apaf-1*$^{+/+}$ and the *Apaf-1*$^{-/-}$ thymuses (Figure 4b). These results indicated that the thymocytes at E14.5 could activate caspase-3 and CAD using an Apaf-1-independent mechanism.

The E17.5 *Apaf-1*$^{-/-}$ thymus also carried DAPI-positive foci (Figure 4c). But, in contrast to the E14.5 *Apaf-1*$^{-/-}$ thymus, the TUNEL reactivity of the foci in the E17.5 *Apaf-1*$^{-/-}$ *DNase II*$^{-/-}$ *IFN-IR*$^{-/-}$ thymus was very weak, and processed caspase-3 was barely detected. Staining with F4/80 indicated that the DAPI-positive foci in the *Apaf-1*$^{-/-}$ thymus were inside macrophages (Figure 4c), and the electron microscopy showed that the DNA that accumulated in the macrophages was intact (Figure 4d). These properties of the E17.5 *Apaf-1*$^{-/-}$ thymus were different from those of the E14.5 thymus, but

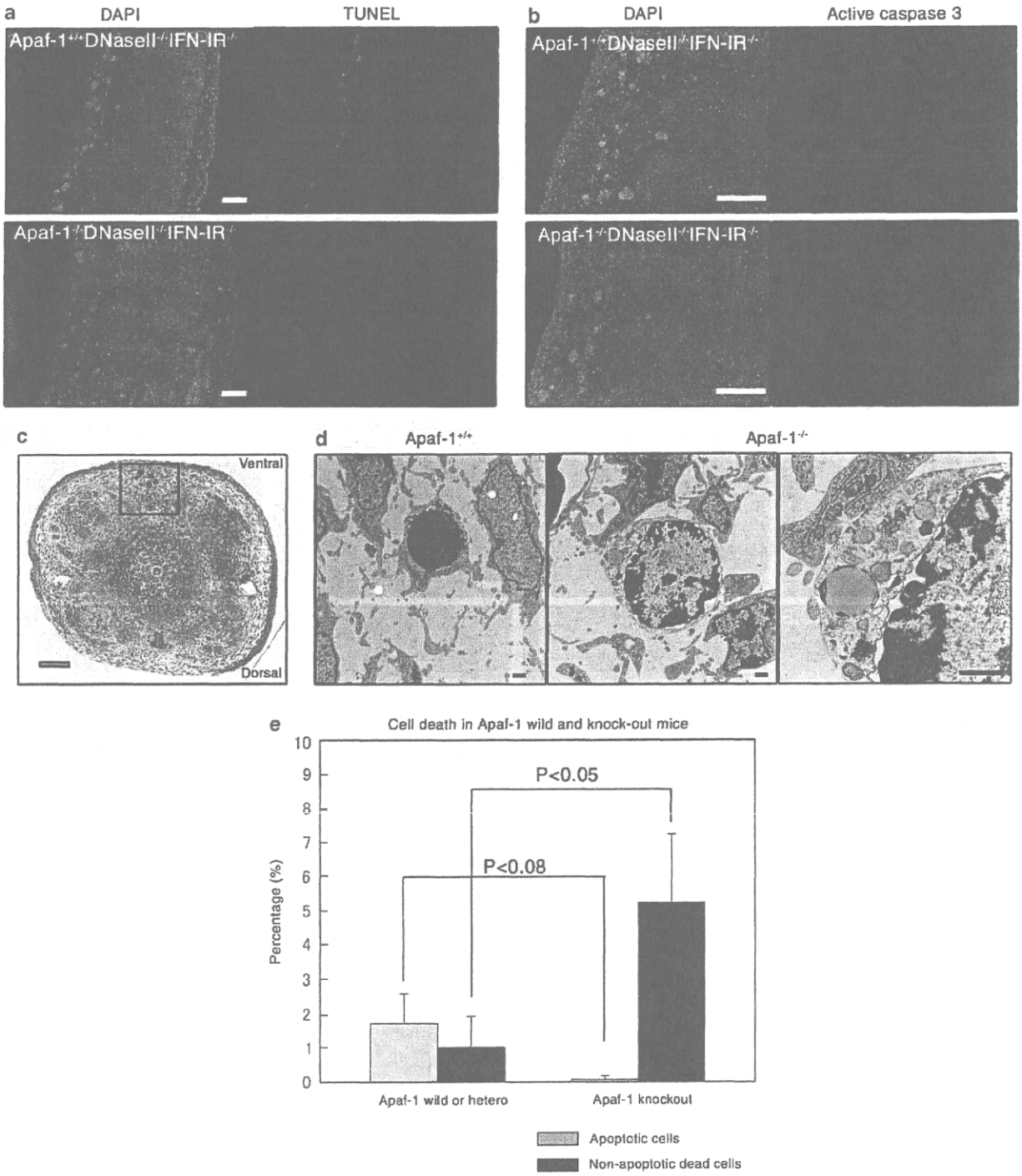

Figure 3 Apaf-1-independent nonapoptotic cell death. (**a–c**) Programmed cell death in the tail. Paraffin sections (**a**) or cryosections (**b**) of the tail from E14.5 *Apaf-1*$^{+/+}$ *DNase II*$^{-/-}$ *IFN-IR*$^{-/-}$ (upper) and *Apaf-1*$^{-/-}$ *DNase II*$^{-/-}$ *IFN-IR*$^{-/-}$ (lower) embryos were stained with DAPI and TUNEL (**a**), and with DAPI and a rabbit mAb against processed caspase-3 (**b**). Scale bar = 100 μm. In (**c**), a transverse section of the tail from an *Apaf-1*$^{+/-}$ *DNase II*$^{-/-}$ *IFN-IR*$^{-/-}$ embryo at E14.5 was stained with toluidine blue. Scale bars = 100 μm. (**d**) Electron microscopy. Sections from the E14.5 tail of *Apaf-1*$^{+/+}$ *DNase II*$^{+/-}$ *IFN-IR*$^{-/-}$ (left) and *Apaf-1*$^{-/-}$ *DNase II*$^{+/+}$ *IFN-IR*$^{-/-}$ (middle and right) embryos were analyzed by electron microscopy. Apoptotic cells in the *Apaf-1*$^{+/+}$ embryos (left) and nonapoptotic dead cells (middle and right) in the *Apaf-1*$^{-/-}$ embryos are shown. Arrowheads indicate dilated mitochondria. Scale bar = 1 μm. (**e**) Increase in nonapoptotic dead cells in the *Apaf-1*$^{-/-}$ tail. Electron micrographs (55 × 55 μm) with low magnification of the ventral parts (boxed area in **c**) of the tail of *Apaf-1*$^{+/+}$ or $^{+/-}$ and *Apaf-1*$^{-/-}$ embryos at E14.5 were assembled, and the percentages of apoptotic and nonapoptotic dead cells out of 950 cells were determined. Average numbers obtained from three embryos are plotted

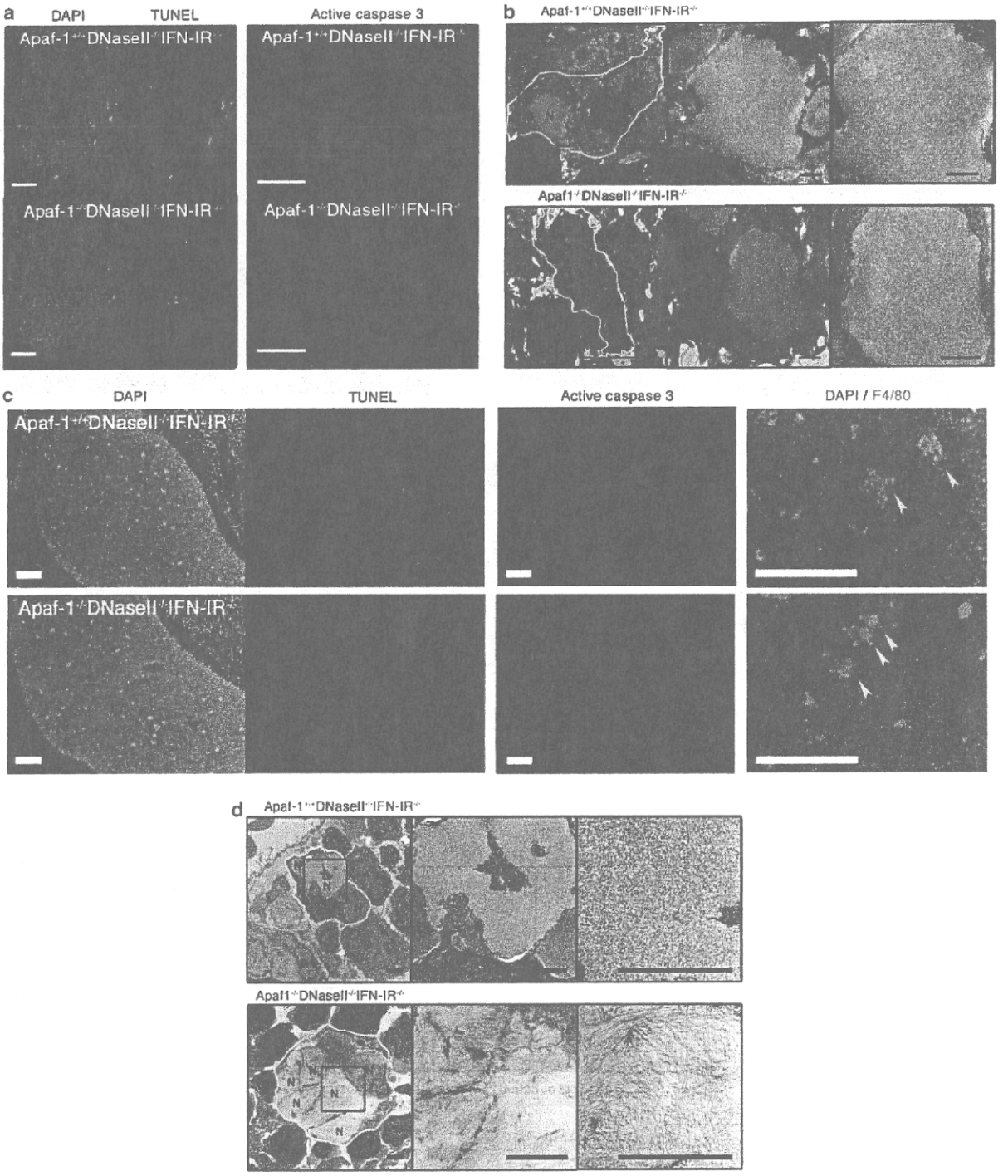

Figure 4 Programmed cell death in the fetal thymus. (**a**) Programmed cell death at E14.5. Paraffin sections (left) or cryosections (right) of the thymus from E14.5 *Apaf-1*$^{+/+}$ *DNase II*$^{-/-}$ *IFN-IR*$^{-/-}$ (upper) and *Apaf-1*$^{-/-}$ *DNase II*$^{-/-}$ *IFN-IR*$^{-/-}$ (lower) embryos were stained with DAPI and TUNEL using the digoxigenin/anti-digoxigenin fluorescein system (left), or with an anti-processed caspase-3 mAb (right). Scale bars = 100 μm. (**b**) Electron microscopy of the E14.5 thymus. Sections from the thymus of E14.5 *Apaf-1*$^{+/+}$ *DNase II*$^{-/-}$ *IFN-IR*$^{-/-}$ (upper) and *Apaf-1*$^{-/-}$ *DNase II*$^{-/-}$ *IFN-IR*$^{-/-}$ (lower) embryos were analyzed by electron microscopy. Boxed areas were enlarged. N, nuclear DNA from the engulfed dead cells; MN, macrophage nuclei. Scale bar = 1 μm. (**c**) Programmed cell death at E17.5. Adjacent cryosections of the thymus from E17.5 embryos with *Apaf-1*$^{+/+}$ *DNase II*$^{-/-}$ *IFN-IR*$^{-/-}$ (upper) and *Apaf-1*$^{-/-}$ *DNase II*$^{-/-}$ *IFN-IR*$^{-/-}$ (lower) embryos were stained with DAPI and TUNEL (left), or with an anti-processed caspase-3 mAb. Scale bars = 100 μm. In the right, the sections were stained with DAPI and a rat mAb against mouse F4/80, and their staining profiles were merged. Yellow arrowheads indicate the macrophages carrying engulfed DNA. Scale bar = 100 μm. (**d**) Electron microscopy of the E17.5 thymus. Sections from the E17.5 thymus of *Apaf-1*$^{+/+}$ *DNase II*$^{-/-}$ *IFN-IR*$^{-/-}$ (upper) and *Apaf-1*$^{-/-}$ *DNase II*$^{-/-}$ *IFN-IR*$^{-/-}$ (lower) embryos were analyzed by electron microscopy. Boxed areas in the left panels were enlarged in the adjacent right panels. N, nuclear DNA from the engulfed dead cells; MN, macrophage nuclei. Scale bars = 2 μm

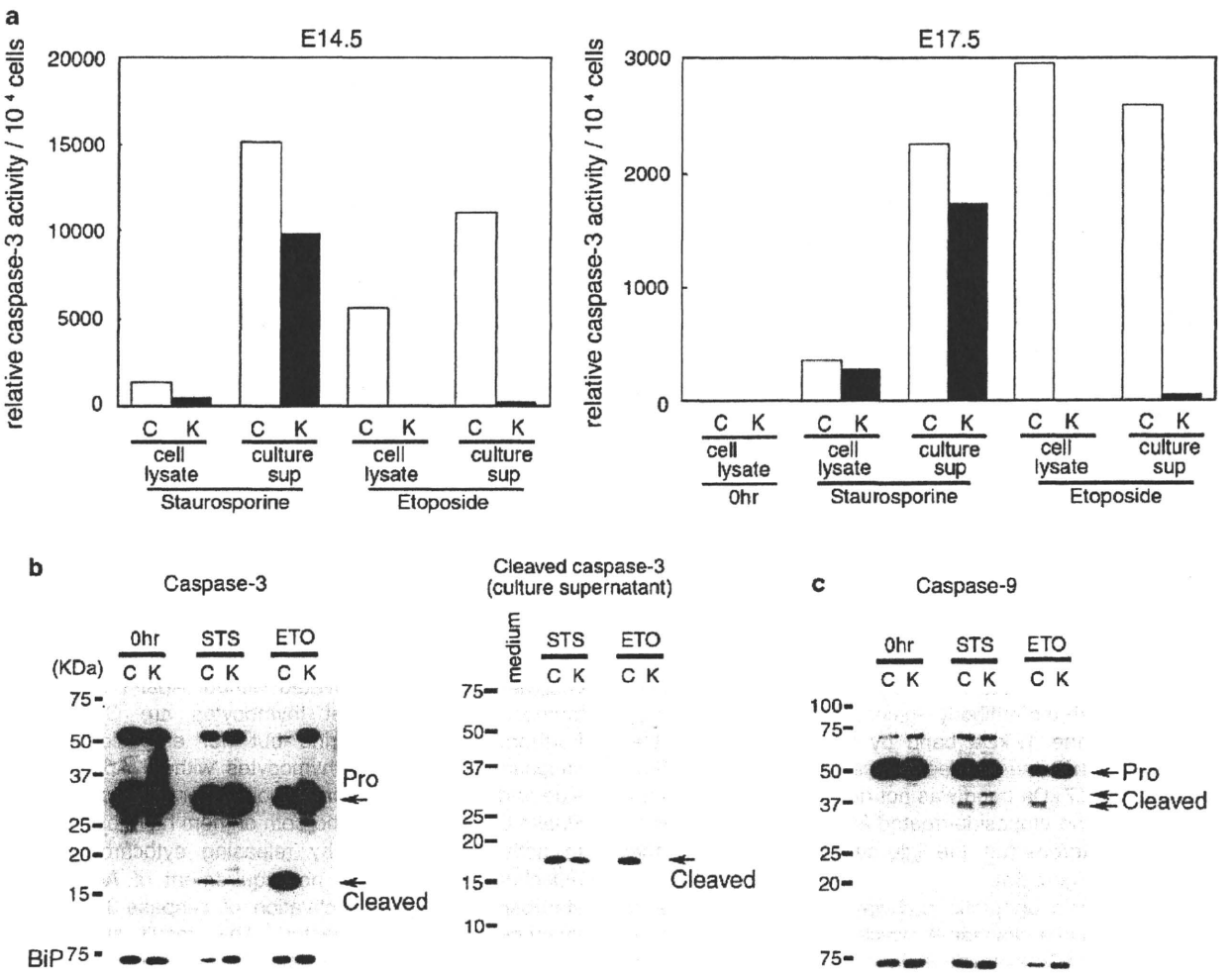

Figure 5 Apaf-1-independent caspase activation. (**a**) Activation of caspase-3. Thymocytes were prepared from E14.5 or E17.5 embryos with *Apaf-1*$^{+/+}$ or *Apaf-1*$^{+/-}$ (C) and *Apaf-1*$^{-/-}$ (K) genotypes, and treated with 10 μM staurosporine or 50 μM etoposide for 4 h. The caspase activity in the cell lysates and supernatant was determined with Ac-DEVD-AMC as described in Materials and Methods. The caspase activity is expressed in an arbitrary unit. One ng recombinant human caspase-3 gave 14 100 U under the same conditions. Experiments were performed twice with different fetal thymus, and the average values are shown. (**b**) Processing of caspase-3. In left panel, thymocytes from E17.5 embryos with *Apaf-1*$^{+/+}$ or *Apaf-1*$^{+/-}$ (C) and *Apaf-1*$^{-/-}$ (K) genotypes were treated with 10 μM staurosporine (STS) for 2 h or with 50 μM etoposide (ETO) for 4 h, and the cell lysates were subjected to western blotting with rabbit mAb against mouse caspase-3. The cell lysates from untreated thymocytes were also analyzed (0 h). Bands for the proform and cleaved form of caspase-3 are indicated by arrows. As a loading control, the membrane was re-blotted for BiP, and shown in the bottom. In right panel, thymocytes were treated for 4 h with staurosporine (STS) or etoposide (ETO). The supernatant was immunoprecipitated with rabbit mAb against the cleaved caspase-3, and subjected to western blotting with the same mAb, followed by incubation with HRP-conjugated Protein A. The bands for cleaved caspase-3 are indicated by an arrow. (**c**) Processing of caspase-9. Thymocytes from E17.5 embryos with *Apaf-1*$^{+/+}$ or *Apaf-1*$^{+/-}$ (C) and *Apaf-1*$^{-/-}$ (K) genotypes were treated 10 μM staurosporine (STS) for 2 h or with 50 μM etoposide (ETO) for 4 h. The cell lysates from the STS- and ETO-treated and untreated (0 h) thymocytes were subjected to western blotting with mouse mAb against mouse caspase-9. Bands for the proform and cleaved form of caspase-9 are indicated by arrows. The membrane was re-blotted for BiP, and is shown in the bottom

similar with those found in other tissues (interdigits, and tail) at E14.5 and 17.5.

Apaf-1-independent caspase activation. To examine whether thymocytes can undergo caspase-dependent apoptotic cell death in the absence of Apaf-1, we prepared thymocytes from the wild-type and *Apaf-1*$^{-/-}$ E14.5 embryos. They were treated with two different apoptosis inducers, etoposide and staurosporine, and the caspase-3 activity in the cell lysates was determined with a fluorescent substrate, Ac-DEVD-AMC. As shown in Figure 5a, a strong caspase-3 activity (about 5600 U) could be detected in the cell lysates from the wild-type but not *Apaf-1*-deficient thymocytes treated with 50 μM etoposide. The cell lysates from the thymocytes treated with 10 μM staurosporine also showed a caspase-3-activity (about 1300 U). Different from the treatment with etoposide, the cell lysates from the staurosporine-treated *Apaf-1*$^{-/-}$ thymocytes carried a significant caspase-3 activity (500 U). The active caspase-3 is often released from the cells into supernatant.[27] In fact, the supernatant from

staurosporine-treated *Apaf-1*$^{+/+}$ and *Apaf-1*$^{-/-}$ thymocytes carried a high caspase-3 activity (10 000–15 000 U). Conversely, the treatment with etoposide produced the caspase-3 activity in the supernatant with *Apaf-1*$^{+/+}$ thymocytes, but not with *Apaf-1*$^{-/-}$ thymocytes. These results indicated that etoposide could activate caspase-3 in E14.5 thymocytes in an Apaf-1-dependent manner, whereas Apaf-1 is dispensable for the staurosporine-induced activation of caspase-3. Similar results were obtained with E17.5 thymocytes, that is, staurosporine but not etoposide activated caspase-3 in E17.5 *Apaf-1*$^{-/-}$ thymocytes as efficiently as *Apaf-1*$^{+/+}$ thymocytes, although the extent of the activated caspase-3 per cell is significantly lower than that found with E14.5 thymocytes (Figure 5a).

To confirm the caspase-3 activity detected with Ac-DEVD-AMC is due to the processed caspase-3, we analyzed the cell lysates using western blot method with the antibody against caspase-3. As shown in Figure 5b, the lysates from the staurosporine-treated *Apaf-1*$^{+/+}$ and *Apaf-1*$^{-/-}$ thymocytes showed a 17 kDa band for the processed caspase-3. This band was detected in the lysates from the etoposide-treated *Apaf-1*$^{+/+}$ but not *Apaf-1*$^{-/-}$ thymocytes, and its intensity correlated with the caspase-3 activity detected (Figure 5a). When the culture supernatants from staurosporine- or etoposide-treated E17.5 *Apaf-1*$^{+/+}$ thymocytes were immunoprecipitated with the antibody against processed caspase-3, they showed the 17 kDa band by western blot with the antibody against the processed caspase-3 (Figure 5b). However, the 17 kDa band was not detected in the immunoprecipitate of the etoposide-treated E17.5 *Apaf-1*$^{-/-}$ thymocytes, which agrees with the little caspase-3 activity in the supernatant (Figure 5a).

In the intrinsic apoptotic pathway, Apaf-1 works as a scaffold to activate caspase-9, which induces processing of procaspase-3.[10] To examine an involvement of caspase-9 in the Apaf-1-independent activation of caspase-3, we carried out western blot analysis with anticaspase-9. As shown in Figure 5c, the 37 kDa processed caspase-9 could be detected in the lysates from the staurosporine-treated *Apaf-1*$^{+/+}$ as well as *Apaf-1*$^{-/-}$ thymocytes. In contrast, the processing of procaspase-9 in the etoposide-treated thymocytes was observed in the *Apaf-1*$^{+/+}$ thymocytes, but not in the *Apaf-1*$^{-/-}$ thymocytes. These results indicate that staurosporine but not etoposide can activate caspase-9 in the absence of Apaf-1.

Discussion

Many cells die during mammalian development. However, as the dead cells are swiftly engulfed by macrophages for degradation, it is difficult to detect them. For example, more than 90% of thymocytes undergo programmed cell death during the development of the thymus. But, only a small percentage of the cells can be stained by TUNEL at a given time point.[28] Many neurons also undergo programmed cell death in the brain, but the reported number differs greatly among researchers,[29–31] probably due to the difficulty in detecting dead cells that are quickly eliminated. Here, we used *DNase II*-null mice to detect the programmed cell death that occurs during mouse embryogenesis. The *DNase II*-null mice carried in various tissues macrophages that contained undigested DNA, suggesting that cells died surrounding the macrophages and were engulfed. Although it is difficult to determine which and how many cells died, the *DNase II*$^{-/-}$ mice were nonetheless useful for localizing the regions where programmed cell death occurs. The macrophages carrying undigested DNA eventually disappeared, probably because those with a heavy load of DNA could not survive, suggesting that the *DNase II*$^{-/-}$ mice can also be used to estimate the time when programmed cell death takes place. In fact, we have been able to show that specific layers of cerebral neurons undergo programmed cell death at specific stages of mouse embryogenesis (AN, KK, and SN, manuscript in preparation).

Crossing the *Apaf-1*$^{-/-}$ mice with *DNase II*$^{-/-}$ mice, we showed that most of the apoptotic cell death during mouse embryonic development takes place through an Apaf-1-dependent pathway. This agrees with previous reports that deletion of the *Apaf-1* or *caspase-9* gene blocks apoptotic cell death in the brain, and ear.[13,14] Similarly, the apoptotic cell death in E17.5 thymus was also blocked by deficiency of *Apaf-1*, indicating that the negative and positive selections at CD4$^+$CD8$^+$ thymocytes proceed in an Apaf-1-dependent pathway. In contrast, very surprisingly, we found that caspase-3 could be activated without Apaf-1 in the E14.5 thymus, in which most thymocytes are CD4$^-$CD8$^-$.[32] Furthermore, staurosporine but not etoposide activated caspase-3 in the fetal thymocytes without Apaf-1. Etoposide and staurosporine are inhibitors for topoisomerase and kinase C, respectively, and both of them have been reported to activate caspase-3 by releasing cytochrome *c* from mitochondria.[33,34] Thus, no requirement of Apaf-1 in the staurosporine-induced activation of caspase-3 in the fetal thymocytes was unexpected. This result suggests that staurosporine can activate caspase-3 in thymocytes through a pathway that does not use cytochrome *c*, and this pathway may be similar to that used in the Apaf-1-independent apoptotic cell death of E14.5 thymocytes. We observed that caspase-3 can be activated without Apaf-1 not only in the fetal thymus but also in the fetal liver (AN, KK, and SN, unpublished observation), which may be consistent with reports that hemopoietic cells reconstituted with fetal liver cells can activate caspase without Apaf-1.[18,35,36] To understand this apoptosis, it will be necessary to determine how and which caspases are activated by staurosporine without Apaf-1.

Even when the caspase was not activated in *Apaf-1*-deficient mice, macrophages carrying undigested DNA were present in the embryo, in particular at the late stage of development, indicating that cells could die without Apaf-1, and were engulfed by macrophages. This agrees with the previous report showing that myeloid cells die without Apaf-1 or caspase-9.[37] Several Apaf-1- or caspase-independent cell death processes have been proposed, including autophagic cell death and necrosis.[38] As reported for the interdigits of *Apaf-1*$^{-/-}$ embryos,[39] we found in the ectodermal ridge of the tails of *Apaf-1*$^{-/-}$ mice many cells exhibiting mottled chromatin condensation, nuclear membrane detachment and rupture, and dilated mitochondria. Whereas, no cells with the characteristics of autophagy (double-membraned vacuoles), indicating that the cells probably died because of necrosis.

One possible cause of nonapoptotic cell death is that the stimuli that induce programmed cell death in mouse embryogenesis cause cytochrome *c* to be released, inactivating mitochondrial function, which leads to cell death.[37] The mice lacking both Bak and Bax that are essential for the release of cytochrome *c*[40] show the persistence of interdigital webs,[17] which suggests that Bak/Bax can cause necrotic cell death by releasing cytochrome *c*. It will be interesting to examine whether the null mutation of *Bax* and *Bak* can prevent the generation of macrophages carrying undigested DNA in *DNase II*-null embryos.

In *Apaf-1*$^{-/-}$ embryos, dead cells were found in macrophages, indicating that the nonapoptotic dead cells were recognized by macrophages for engulfment. In *C. elegans*, a common set of genes mediates the removal of both apoptotic and necrotic cell corpses.[41] Conversely, different mechanisms have been proposed to clear apoptotic and necrotic cells in mammalian system.[42] Apoptotic cells expose phosphatidylserine, which is recognized by specific receptors or opsonins for engulfment.[12] Because necrotic cells also expose phosphatidylserine at a late stage,[38] it is possible that similar receptors or opsonins mediate the engulfment of apoptotic and necrotic cells. The complement system is another candidate for the engulfment of late apoptotic or necrotic cells.[43] It will be interesting to study the engulfment of necrotic cells by crossing the *Apaf-1*$^{-/-}$ mice with mice deficient in the engulfment of apoptotic or necrotic cells.[44,45] Unengulfed apoptotic cells are difficult to find in mouse tissues. However, we frequently detected unengulfed dead cells with nonapoptotic morphology in the *Apaf-1*$^{-/-}$ embryos, suggesting that the engulfment of nonapoptotic dead cells is inefficient compared with that of apoptotic cells. This may allow noxious materials to be released from dying cells. In addition, the engulfment of necrotic cells but not apoptotic ones is known to cause the release of inflammatory cytokines.[46] In this regard, it will be interesting to study whether the normally developing *Apaf-1*$^{-/-}$ mice suffer from inflammatory disease.

Materials and Methods

Mice. C57BL/6 mice were purchased from Nippon SLC (Hamamatsu, Japan) or Shimizu Laboratory (Kyoto, Japan) Supplies. *DNase II*$^{-/-}$ mice[20] were backcrossed to C57BL/6 at lease six times. *IFN-IR*$^{-/-}$ mice[47] in the C57BL/6 background were obtained from Michel Aguet (Swiss Institute for Experimental Cancer Research, Epalinges, Switzerland). *Apaf-1*$^{-/-}$ mice in the C57BL/6 background were described previously.[14,19] *DNase II*$^{-/-}$*IFN-IR*$^{-/-}$ mice and *Apaf-1*$^{-/-}$*DNase II*$^{-/-}$*IFN-IR*$^{-/-}$ embryos were generated by crossing *Apaf-1*$^{+/-}$*DNase II*$^{-/-}$*IFN-IR*$^{-/-}$ parents, respectively. Mice were housed in specific pathogen-free facilities at Osaka University Medical School and Oriental Bio Service. All animal experiments were conducted according to the Guidelines for Animal Experiments of Osaka University or Kyoto University. To determine the genotype of *DNase II* and *IFN-IR* alleles, we prepared DNA from embryonic tissues or adult tail-snip tissue, as described,[48] and analyzed using PCR. For the *DNase II* gene, a sense primer specific for the wild-type (5′-GCCCATCTAGACTAACTTTC-3′) or mutant allele (5′-GATTCGCAGCGCATCG CCTT-3′); sequence in the neomycin-resistant gene) was used with a common antisense primer (5′-GAGTCTTAGTCCTTTGCTCCG-3′). The wild-type and mutant alleles for *IFN-IR* were examined with a wild-type (5′-AAGATGTGCTGTTCCC TTCCTCTGCTCTGA-3′) or mutant-specific (5′-CCTGCGTGCAATCCATCTTG-3′) antisense primer and a common sense primer (5′-ATTATTAAAAGAAAAGACGA GGCGAAGTGG-3′). For the *Apaf-1* allele, a wild-type (5′-CTCAAACACCTCCTCC ACAA-3′) or mutant-specific (5′-GGGCCAGCTCATTCCTC-3′) sense primer was used with a common antisense primer (5′-GTCATCTGGAAGGGCAGCGA-3′).

Histochemical analysis with paraffin sections. Embryos were fixed with 4% PFA in 0.1 M Na-phosphate buffer (pH 7.2) containing 4% sucrose at 4°C for more than 1 day with shaking. They were gradually dehydrated by dipping into 50, 70, 80, and 90% ethanol at room temperature for 12 h each, and then twice in 100% ethanol for 1 h. The samples were soaked twice in 100% xylene at room temperature for 1 h, in a 1 : 1 mixture of xylene and paraffin for 2 h at 60°C. They were embedded in paraffin by successive incubations in paraffin for 12 and 4 h at 60°C, and sectioned at 4 μm using a microtome (RM2245; Leica, Solms, Germany).

For TUNEL staining, sections were treated at room temperature for 20 min with 20 μg/ml Proteinase K, and stained with an Apoptag kit (Millipore, Bedford, MA, USA), according to the manufacturer's instructions, except that the amount of terminal transferase was reduced to 10% of the recommended concentration. Sections were mounted with Mount-Quick (Daido Sangyo, Toda, Saitama, Japan) or Fluoromount (Diagnostic BioSystems, Pleasanton, CA, USA), and observed by fluoroescence microscopy (IX-70; Olympus, Tokyo, Japan or BioRevo BZ-9000; Keyence, Osaka, Japan).

Histochemical analysis with cryosections. Embryos were fixed at 4°C in 4% PFA containing 4% sucrose in 0.1 M Na-phosphate buffer (pH 7.2) for 2 h, successively immersed in 10 and 20% sucrose-containing 0.1 M Na-phosphate buffer (pH 7.2) for 4 h and overnight each, embedded in OCT compound (Sakura Finetek, Tokyo, Japan), and frozen in liquid nitrogen. Sections (10 μm) were prepared using a cryostat (CM3050 S; Leica) in the cold (−16 to −25°C).

To detect active caspase-3, we fixed sections with 4% PFA in PBS at room temperature for 10 min, and blocked with 5% normal goat serum in PBS containing 0.3% Triton X-100 at room temperature for 1 h. They were stained at 4°C overnight with a 100-fold diluted rabbit monoclonal antibody (mAb) against active caspase-3 (clone 5A1E; Cell Signaling, Danvers, MA, USA), followed by incubation at room temperature for 1 h with Cy3-conjugated goat anti-rabbit IgG (Jackson Laboratories, West Grove, PA, USA).

For the staining of F4/80 antigen, a rat hybridoma against mouse F4/80[49] was grown in serum-free GIT medium (Nihon Pharmaceutical, Tokyo, Japan). Cryosections from mouse embryos were fixed at room temperature for 10 min with 1% PFA in PBS. After blocking with 10% normal rabbit serum and 0.5% BSA in PBS at room temperature for 1 h, sections were incubated at 4°C overnight with the supernatant of the F4/80 hybridoma, and washed with PBS containing 0.5% BSA. The endogenous peroxidase was quenched by incubation at 4°C for 20–30 min with 3% H_2O_2 in methanol, and incubated at room temperature for 45 min with peroxidase-conjugated rabbit anti-rat Ig (Dako, Copenhagen, Denmark). The signals were detected by incubation at room temperature for 5 min with Cy3-labeled tyramide (PerkinElmer, Boston, MA, USA).

TUNEL staining was performed as described above, except that the concentration of terminal transferase was reduced to 0.4–0.5% of that recommended by the manufacturer. Sections were mounted with mounting reagent containing 1–2 μg/ml DAPI (Dojin Laboratories, Kumamoto, Japan), and observed by microscopy as described earlier.

Electron microscopy. Embryonic tissues were fixed by incubation at 4°C for 2 h in 0.1 M Na-phosphate buffer (pH 7.2) containing 2% PFA and 2% glutaraldehyde. After being washed five times with 0.1 M Na-phosphate buffer (pH 7.2) at 4°C for 20 min each, the samples were post-fixed at 4°C for 2 h with 1% OsO_4 in the same buffer, and dehydrated at 4°C by dipping into a graded series (50, 60, 70, 80, 90, 99%) of ethanol for 10 min each. After two 20-min immersions in 100% ethanol, the samples were incubated at 35°C twice in propylene oxide for 20 min, in a 3 : 1 mixture of propylene oxide and epoxide for 1 h, in a 1 : 3 mixture of propylene oxide and epoxide for 1 h, and in epoxide overnight. They were then embedded in epoxide by incubation at 60°C for 3 days. Ultrathin sections (80–90 nm) were prepared with an ultramicrotome (Ultracut N; Reichert-Nissei, Kumamoto, Japan), stained with uranyl acetate and lead citrate, and observed with a Hitachi H-7650 microscope (Hitachi High-Technologies, Tokyo, Japan).

Assay for caspase-3. Thymocytes (4×10^4 cells per 100 μl) from E14.5 embryos or thymocytes (5×10^5 cells per 200 μl) from E17.5 embryos were treated with 10 μM staurosporine or 50 μM etoposide in DMEM containing 10% FCS. The caspase-3 activity in the cell lysates and medium was determined using Caspase-3 Cellular Assay Kit PLUS (Enzo Life Sciences, Farmingdale, NY, USA) according to the instructions provided by the manufacturer. In brief, cells were collected by centrifugation at 5000 r.p.m. for 5 min, washed with PBS, and lysed with 50 μl Lysis Buffer (50 mM HEPES-NaOH buffer (pH 7.4), 0.1% CHAPS, 5 mM DTT, and

0.1 mM EDTA). Aliquots (10 μl) of the medium or cell lysates were incubated at 37°C for 3 h with 30 μM Ac-DEVD-AMC in 100 μl Assay Buffer (50 mM HEPES-NaOH buffer (pH 7.4), 100 mM NaCl, 0.1% CHAPS, 10 mM DTT, 1 mM EDTA, and 10% glycerol), and the fluorescence was detected with an excitation wavelength of 360 nm and emission wavelength of 460 using a microplate reader (Infinite M200; Tecan, Männedorf, Switzerland). The specific caspase-3 activities were determined by subtracting the values obtained in the presence of 0.1 μM Ac-DEVD-CHO.

Western blot analysis. For western blotting, cells (5×10^5) were directly lysed by heating at 85°C for 30 min in 15 μl of sample buffer (30 mM Tris-HCl (pH 6.8), 1% SDS, 5% glycerol, 2.5% 2-mercaptoethanol, and 0.0005% BPB). Proteins were separated by 10–20% gradient SDS–PAGE, and transferred to PVDF membranes (Millipore). After blocking with blocking buffer (Tris-buffered saline containing 0.05% Tween 20 (TBST) supplemented with 5% non-fat dry milk or 4% Block Ace (DS Pharma Biomedical, Suita, Osaka, Japan)), the membranes were incubated at 4°C overnight with rabbit mAb against caspase-3 (clone 8G10; Cell Signaling) or mouse mAb against caspase-9 (clone 5B4; MBL, Nagoya, Japan) in blocking buffer. After washing with TBST, the membranes were incubated with HRP-conjugated anti-rabbit Ig or anti-mouse Ig antibody at room temperature for 1 h, and the proteins recognized by the antibody were visualized by a chemiluminescence reaction (Immobilon Western, Millipore). Western blotting with mouse mAb against BiP (Grp78) (clone 40; BD Biosciences) was performed as a loading control.

For immunoprecipitation, the culture supernatant was precleared by incubating twice at 4°C with a 1 : 1 mixture of nProtein A-Sepharose 4 Fast Flow (GE Healthcare, Uppsala, Sweden) and Protein G-Sepharose 4 Fast Flow (GE Healthcare) for 1.5 h. After removing Sepharose by centrifugation, the supernatant was incubated at 4°C overnight with rabbit mAb against the cleaved caspase-3 (clone 5A1E; Cell Signaling), followed by the incubation with Protein A-Sepharose. After washing with PBS containing 1% Triton X-100, the proteins bound to the beads were eluted by boiling in SDS sample buffer, separated by 10–20% SDS–PAGE, transferred onto a PVDF membrane, and subjected to western blotting with rabbit mAb against the cleaved caspase-3, followed by the incubation with HRP-conjugated Protein A (Bio-Rad, Hercules, CA, USA).

Conflict of interest

The authors declare no conflict of interest.

Acknowledgements. We thank Dr. M Koike (Juntendo University) for his advice for the immunochemical staining, and M Fujii and M Harayama for secretarial assistance. This work was supported in part by Grants-in-Aid from the Ministry of Education, Science, Sports, and Culture in Japan, and by the Kyoto University Global COE Program (Center for Frontier Medicine). AN was a research assistant for the Osaka University Global COE Program (System Dynamics of Biological Function).

1. Jacobson MD, Weil M, Raff MC. Programmed cell death in animal development. *Cell* 1997; **88**: 347–354.
2. Vaux DL, Korsmeyer SJ. Cell death in development. *Cell* 1999; **96**: 245–254.
3. Kerr JF, Wyllie AH, Currie AR. Apoptosis: a basic biological phenomenon with wide-ranging implications in tissue kinetics. *Br J Cancer* 1972; **26**: 239–257.
4. Adams JM. Ways of dying: multiple pathways to apoptosis. *Genes Dev* 2003; **17**: 2481–2495.
5. Danial NN, Korsmeyer SJ. Cell death: critical control points. *Cell* 2004; **116**: 205–219.
6. Nagata S. Apoptosis by death factor. *Cell* 1997; **88**: 355–365.
7. Strasser A, Jost PJ, Nagata S. The many roles of FAS receptor signaling in the immune system. *Immunity* 2009; **30**: 180–192.
8. Nagata S. DNA degradation in development and programmed cell death. *Annu Rev Immunol* 2005; **23**: 853–875.
9. Jiang X, Wang X. Cytochrome c-mediated apoptosis. *Annu Rev Biochem* 2004; **73**: 87–106.
10. Schafer ZT, Kornbluth S. The apoptosome: physiological, developmental, and pathological modes of regulation. *Dev Cell* 2006; **10**: 549–561.
11. Fadok VA, Bratton DL, Frasch SC, Warner ML, Henson PM. The role of phosphatidylserine in recognition of apoptotic cells by phagocytes. *Cell Death Differ* 1998; **5**: 551–562.
12. Ravichandran KS, Lorenz U. Engulfment of apoptotic cells: signals for a good meal. *Nat Rev Immunol* 2007; **7**: 964–974.
13. Kuida K, Haydar TF, Kuan CY, Gu Y, Taya C, Karasuyama H *et al.* Reduced apoptosis and cytochrome c-mediated caspase activation in mice lacking caspase 9. *Cell* 1998; **94**: 325–337.
14. Yoshida H, Kong YY, Yoshida R, Elia AJ, Hakem A, Hakem R *et al.* Apaf1 is required for mitochondrial pathways of apoptosis and brain development. *Cell* 1998; **94**: 739–750.
15. Hao Z, Duncan GS, Chang CC, Elia A, Fang M, Wakeham A *et al.* Specific ablation of the apoptotic functions of cytochrome *c* reveals a differential requirement for cytochrome *c* and Apaf-1 in apoptosis. *Cell* 2005; **121**: 579–591.
16. Cecconi F, Alvarez-Bolado G, Meyer BI, Roth KA, Gruss P. Apaf1 (CED-4 homolog) regulates programmed cell death in mammalian development. *Cell* 1998; **94**: 727–737.
17. Lindsten T, Ross AJ, King A, Zong WX, Rathmell JC, Shiels HA *et al.* The combined functions of proapoptotic Bcl-2 family members bak and bax are essential for normal development of multiple tissues. *Mol Cell* 2000; **6**: 1389–1399.
18. Marsden VS, O'Connor L, O'Reilly LA, Silke J, Metcalf D, Ekert PG *et al.* Apoptosis initiated by Bcl-2-regulated caspase activation independently of the cytochrome *c*/Apaf-1/caspase-9 apoptosome. *Nature* 2002; **419**: 634–637.
19. Okamoto H, Shiraishi H, Yoshida H. Histological analyses of normally grown, fertile Apaf1-deficient mice. *Cell Death Differ* 2006; **13**: 668–671.
20. Kawane K, Fukuyama H, Kondoh G, Takeda J, Ohsawa Y, Uchiyama Y *et al.* Requirement of DNase II for definitive erythropoiesis in the mouse fetal liver. *Science* 2001; **292**: 1546–1549.
21. Kawane K, Fukuyama H, Yoshida H, Nagase H, Ohsawa Y, Uchiyama Y *et al.* Impaired thymic development in mouse embryos deficient in apoptotic DNA degradation. *Nat Immunol* 2003; **4**: 138–144.
22. Krieser RJ, MacLea KS, Longnecker DS, Fields JL, Fiering S, Eastman A. Deoxyribonuclease IIalpha is required during the phagocytic phase of apoptosis and its loss causes lethality. *Cell Death Differ* 2002; **9**: 956–962.
23. Wu YC, Stanfield GM, Horvitz HR. NUC-1, a *Caenorhabditis elegans* DNase II homolog, functions in an intermediate step of DNA degradation during apoptosis. *Genes Dev* 2000; **14**: 536–548.
24. Mukae N, Yokoyama H, Yokokura T, Sakoyama Y, Nagata S. Activation of the innate immunity in *Drosophila* by endogenous chromosomal DNA that escaped apoptotic degradation. *Genes Dev* 2002; **16**: 2662–2671.
25. Reddien PW, Horvitz HR. The engulfment process of programmed cell death in *Caenorhabditis elegans*. *Annu Rev Cell Dev Biol* 2004; **20**: 193–221.
26. Yoshida H, Okabe Y, Kawane K, Fukuyama H, Nagata S. Lethal anemia caused by interferon-beta produced in mouse embryos carrying undigested DNA. *Nat Immunol* 2005; **6**: 49–56.
27. Denecker G, Vercammen D, Steemans M, Vanden Berghe T, Brouckaert G, Van Loo G *et al.* Death receptor-induced apoptotic and necrotic cell death: differential role of caspases and mitochondria. *Cell Death Differ* 2001; **8**: 829–840.
28. Surh CD, Sprent J. T-cell apoptosis detected *in situ* during positive and negative selection in the thymus. *Nature* 1994; **372**: 100–103.
29. Verney C, Takahashi T, Bhide PG, Nowakowski RS, Caviness Jr VS. Independent controls for neocortical neuron production and histogenetic cell death. *Dev Neurosci* 2000; **22**: 125–138.
30. Thomaidou D, Mione MC, Cavanagh JF, Parnavelas JG. Apoptosis and its relation to the cell cycle in the developing cerebral cortex. *J Neurosci* 1997; **17**: 1075–1085.
31. Blaschke AJ, Staley K, Chun J. Widespread programmed cell death in proliferative and postmitotic regions of the fetal cerebral cortex. *Development* 1996; **122**: 1165–1174.
32. Rodewald HR, Moingeon P, Lucich JL, Dosiou C, Lopez P, Reinherz EL. A population of early fetal thymocytes expressing Fc gamma RII/III contains precursors of T lymphocytes and natural killer cells. *Cell* 1992; **69**: 139–150.
33. Kaufmann SH. Cell death induced by topoisomerase-targeted drugs: more questions than answers. *Biochim Biophys Acta* 1998; **1400**: 195–211.
34. Maeno E, Ishizaki Y, Kanaseki T, Hazama A, Okada Y. Normotonic cell shrinkage because of disordered volume regulation is an early prerequisite to apoptosis. *Proc Natl Acad Sci USA* 2000; **97**: 9487–9492.
35. Hara H, Takeda A, Takeuchi M, Wakeham AC, Itie A, Sasaki M *et al.* The apoptotic protease-activating factor 1-mediated pathway of apoptosis is dispensable for negative selection of thymocytes. *J Immunol* 2002; **168**: 2288–2295.
36. Matsuki Y, Zhang HG, Hsu HC, Yang PA, Zhou T, Dodd CH *et al.* Different role of Apaf-1 in positive selection, negative selection and death by neglect in foetal thymic organ culture. *Scand J Immunol* 2002; **56**: 174–184.
37. Ekert PG, Read SH, Silke J, Marsden VS, Kaufmann H, Hawkins CJ *et al.* Apaf-1 and caspase-9 accelerate apoptosis, but do not determine whether factor-deprived or drug-treated cells die. *J Cell Biol* 2004; **165**: 835–842.
38. Kroemer G, Galluzzi L, Vandenabeele P, Abrams J, Alnemri ES, Baehrecke EH *et al.* Classification of cell death: recommendations of the Nomenclature Committee on Cell Death 2009. *Cell Death Differ* 2009; **16**: 3–11.
39. Chautan M, Chazal G, Cecconi F, Gruss P, Golstein P. Interdigital cell death can occur through a necrotic and caspase-independent pathway. *Curr Biol* 1999; **9**: 967–970.
40. Wei MC, Zong WX, Cheng EH, Lindsten T, Panoutsakopoulou V, Ross AJ *et al.* Proapoptotic BAX and BAK: a requisite gateway to mitochondrial dysfunction and death. *Science* 2001; **292**: 727–730.

41. Chung S, Gumienny TL, Hengartner MO, Driscoll M. A common set of engulfment genes mediates removal of both apoptotic and necrotic cell corpses in *C. elegans*. *Nat Cell Biol* 2000; **2**: 931–937.
42. Krysko DV, Denecker G, Festjens N, Gabriels S, Parthoens E, D'Herde K *et al*. Macrophages use different internalization mechanisms to clear apoptotic and necrotic cells. *Cell Death Differ* 2006; **13**: 2011–2022.
43. Zwart B, Ciurana C, Rensink I, Manoe R, Hack CE, Aarden LA. Complement activation by apoptotic cells occurs predominantly via IgM and is limited to late apoptotic (secondary necrotic) cells. *Autoimmunity* 2004; **37**: 95–102.
44. Hanayama R, Tanaka M, Miyasaka K, Aozasa K, Koike M, Uchiyama Y *et al*. Autoimmune disease and impaired uptake of apoptotic cells in MFG-E8-deficient mice. *Science* 2004; **304**: 1147–1150.
45. Botto M, Dell'Agnola C, Bygrave AE, Thompson EM, Cook HT, Petry F *et al*. Homozygous C1q deficiency causes glomerulonephritis associated with multiple apoptotic bodies. *Nat Genet* 1998; **19**: 56–59.
46. Fadok VA, Bratton DL, Guthrie L, Henson PM. Differential effects of apoptotic *versus* lysed cells on macrophage production of cytokines: role of proteases. *J Immunol* 2001; **166**: 6847–6854.
47. Muller U, Steinhoff U, Reis LF, Hemmi S, Pavlovic J, Zinkernagel RM *et al*. Functional role of type I and type II interferons in antiviral defense. *Science* 1994; **264**: 1918–1921.
48. Laird PW, Zijderveld A, Linders K, Rudnicki MA, Jaenisch R, Berns A. Simplified mammalian DNA isolation procedure. *Nucleic Acids Res* 1991; **19**: 4293.
49. Austyn JM, Gordon S. F4/80, a monoclonal antibody directed specifically against the mouse macrophage. *Eur J Immunol* 1981; **11**: 805–815.

nature

Vol 460|23 July 2009|doi:10.1038/nature08138

LETTERS

Regulation of the innate immune response by threonine-phosphatase of Eyes absent

Yasutaka Okabe[1,2]†*, Teruyuki Sano[1]* & Shigekazu Nagata[1,2]

Innate immunity is stimulated not only by viral or bacterial components, but also by non-microbial danger signals (damage-associated molecular patterns)[1]. One of the damage-associated molecular patterns is chromosomal DNA that escapes degradation. In programmed cell death and erythropoiesis, DNA from dead cells or nuclei expelled from erythroblasts is digested by DNase II in the macrophages after they are engulfed. *DNase II*$^{-/-}$ (also known as *Dnase2a*$^{-/-}$) mice suffer from severe anaemia or chronic arthritis due to interferon-β (IFN-β) and tumour necrosis factor-α (TNF-α) produced from the macrophages carrying undigested DNA[2,3] in a Toll-like receptor (TLR)-independent mechanism[4]. Here we show that Eyes absent 4 (EYA4), originally identified as a co-transcription factor, stimulates the expression of IFN-β and CXCL10 in response to the undigested DNA of apoptotic cells. EYA4 enhanced the innate immune response against viruses (Newcastle disease virus and vesicular stomatitis virus), and could associate with signalling molecules (IPS-1 (also known as MAVS), STING (TMEM173) and NLRX1). Three groups have previously shown that EYA has phosphatase activity[5–7]. We found that mouse EYA family members act as a phosphatase for both phosphotyrosine and phosphothreonine. The haloacid dehalogenase domain at the carboxy terminus contained the tyrosine-phosphatase, and the amino-terminal half carried the threonine-phosphatase. Mutations of the threonine-phosphatase, but not the tyrosine-phosphatase, abolished the ability of EYA4 to enhance the innate immune response, suggesting that EYA regulates the innate immune response by modulating the phosphorylation state of signal transducers for the intracellular pathogens.

We previously showed that *DNase II*$^{-/-}$ mouse embryonic fibroblasts (MEFs) express CXCL10 and IFN-β when they engulf *Cad*$^{-/-}$ apoptotic cells[4]. We used this system to identify molecules involved in the DNA-induced innate immune response. A MEF complementary DNA library (about 20,000 clones) in a retrovirus-based expression vector was prepared, and divided into 400 pools. Retrovirus was produced for each group (see Methods), and used to infect *DNase II*$^{-/-}$ MEFs. The MEFs were incubated with apoptotic *Cad*$^{-/-}$ thymocytes, and CXCL10 levels in the culture supernatant were quantified. One pool of cDNAs that increased the concentration of CXCL10 from 402 to 1,414 pg ml^{-1} was subjected to sib-selection, which led to the identification of EYA4. When *DNase II*$^{-/-}$ MEFs expressing mouse EYA4 were exposed to apoptotic thymocytes, they produced 3.7- and 25.7-fold more CXCL10 and IFN-β protein, and 8.3- and 11.3-fold more of their transcripts, than the parental cells, respectively (Fig. 1a, b and Supplementary Fig. 1). Overexpressing DNase II in the *DNase II*$^{-/-}$ MEFs blocked the production of CXCL10 and IFN-β, indicating that the effect of EYA4 was on the signal transduction triggered by the undigested DNA.

When wild-type MEFs were transfected with *Escherichia coli* or mammalian DNA, or with polyinosinic-polycytidylic acid (hereafter poly(I:C)), they expressed *Ifnb* messenger RNA[1,8,9] (Fig. 1c). This response was enhanced 6–20-fold by EYA4. When Namalwa cells were infected with Newcastle disease virus (NDV), they expressed IFN-β in a dose-dependent manner (Fig. 1d): the level of IFN-β was 3.8- and 12.1-fold higher in two *Eya4*-expressing clones than in the parental cells. Accordingly, the titre of Vesicular stomatitis virus (VSV) produced in MEFs expressing EYA4 was about 10 times lower than that in the parental MEF (Fig. 1e). When fetal liver macrophages were intracellularly challenged with poly(I:C), they expressed IFN-β, and this was enhanced by EYA4 (Fig. 1f). On the other hand, the expression of IFN-β by the extracellular poly(I:C), lipopolysaccharide (LPS), or CpG oligonucleotide was not enhanced by EYA4. These results indicated that EYA4 specifically enhanced the innate immune response triggered by intracellular sensors. The mammalian EYA family is comprised of four members[10]. The poly(I:C)-induced expression of the *Ifnb* gene was 4–10 times higher in MEFs expressing EYA1, EYA2, EYA3 or EYA4 than in vector-transfected cells (Supplementary Fig. 2). Reduction of EYA expression with a mixture of short-interfering RNAs (shRNAs) against four human *EYA* genes in 293T cells diminished the poly(I:C)-induced *IFNB* expression, and this could be rescued by the expression of mouse EYA4 that does not carry the target sequence for shRNA (Fig. 1g).

Promoters of the *Ifnb* and *Cxcl10* genes carry interferon regulatory element (IRE) and NF-κB sites essential for their expression[11,12]. A deficiency of both *Irf3* and *Irf7* in MEFs completely abrogated the apoptotic-cell-induced production of CXCL10 in EYA4-expressing cells, and co-expression of IRF3 enhanced the effect of EYA4 (Fig. 2a). The poly(I:C)-induced activation of IRF3 (its phosphorylation at Ser 388 (ref. 13) and dimerization[14]), as well as the activation of NF-κB were enhanced by EYA4 (Fig. 2b, c and Supplementary Fig. 3). IPS-1 works as an adaptor[15,16] for the RIG-I (also known as DDX58) and MDA5 (IFIH1) system; MyD88 and TRIF (TICAM1) are adaptors for the TLR system[8]. The IPS-1-mediated activation of the *Ifnb* promoter[15] was 6.1-fold stronger in EYA4-expressing MEFs than in wild-type MEFs. In contrast, the expression of EYA4 had no effect on the MyD88- and TRIF-induced activation of the *Ifnb* promoter (Fig. 2d). When EYA works as a co-transcription factor for the myogenin (*Myog*) gene, it translocates from the cytoplasm to the nucleus[17]. In contrast, EYA4 in MEFs remained in the cytoplasm after stimulation with poly(I:C) (Fig. 2e). When Flag-tagged EYA4, and haemagglutinin (HA)-tagged IPS-1, STING[18] or NLRX1 (refs 19, 20) were expressed in 293T cells, IPS-1, STING and NLRX1 interacted with EYA4 (Fig. 2f and Supplementary Fig. 4). The endogenous IPS-1 interacted with EYA4 transiently after poly(I:C) treatment (Fig. 2g), suggesting that the interaction between EYA4 and IPS-1 is stimulus-dependent.

[1]Department of Medical Chemistry, Graduate School of Medicine, Kyoto University, Yoshida-Konoe, Kyoto 606-8501, Japan. [2]Solution Oriented Research for Science and Technology, and Core Research for Evolutional Science and Technology, Japan Science and Technology Corporation, Kyoto 606-8501, Japan. †Present address: Department of Immunobiology, Yale University School of Medicine, TAC S-669, 300 Cedar Street, New Haven, Connecticut 06510, USA.
*These authors contributed equally to this work.

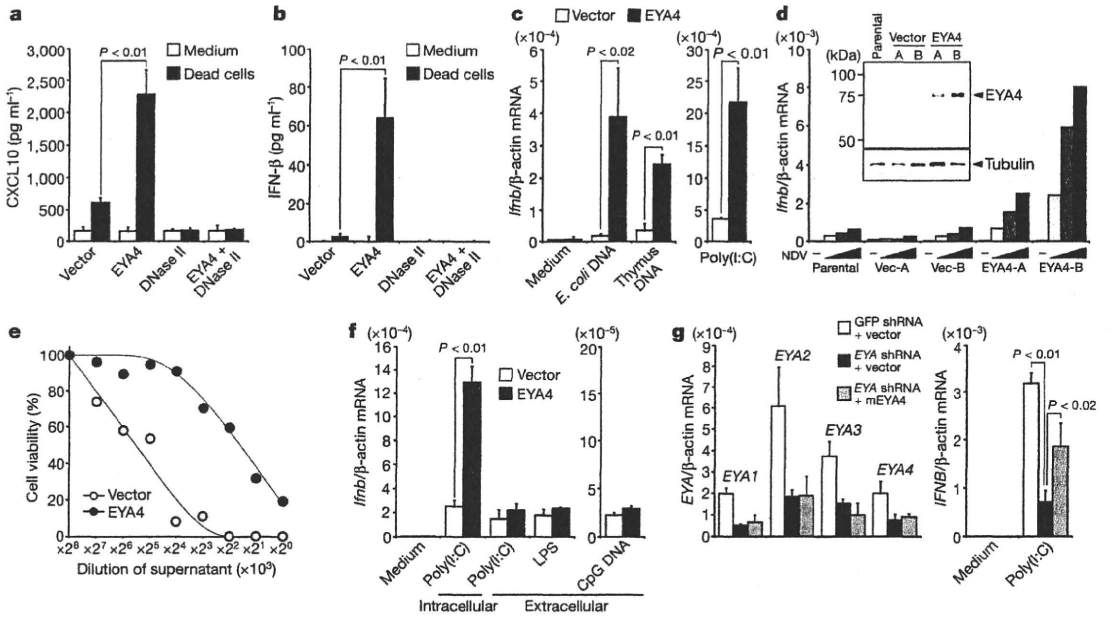

Figure 1 | Identification of EYA4 as a regulator for innate immunity. **a**, **b**, *DNase II*$^{-/-}$ MEFs that expressed EYA4, DNase II, both EYA4 and DNase II, or vector control were incubated with medium or dead cells, and the concentrations of CXCL10 (**a**) and IFN-β (**b**) were quantified. **c**, MEFs plus either vector control or EYA4 were transfected with 100 ng ml^{-1} *E. coli* or calf thymus DNA, or with 10 ng ml^{-1} poly(I:C), and levels of *Ifnb* mRNA were quantified relative to β-actin mRNA levels. **d**, Parental, and vector- or EYA4-Namalwa cells (two clones each, A and B), were challenged with NDV, and *Ifnb* mRNA was quantified at 8 h. Inset, cell lysates were analysed by western blotting. Tubulin was included as a loading control. **e**, MEFs plus vector control or EYA4 were infected with 0.001 multiplicity of infection (m.o.i.) of VSV for 12 h. Cytopathic activity in the supernatants was determined. Values are the means from sextuple samples. **f**, Fetal liver macrophages, infected with EYA4 retrovirus, were transfected with 100 ng ml^{-1} poly(I:C), or extracellularly treated with 100 ng ml^{-1} of poly(I:C), 1.0 ng ml^{-1} LPS, or 1.0 μM CpG, and *Ifnb* mRNA levels were quantified at 6 h. **g**, 293T was transfected with shRNA for GFP, or a mixture of shRNA for human *EYA1–4*, with or without pEF-mEYA4. At 72 h, *EYA* mRNA was quantified (left). The cells were transfected with 1.0 μg ml^{-1} of poly(I:C), and *IFNB* mRNA levels were quantified (right). All error bars are s.d.

To characterize the phosphatase activity of EYA, mouse EYA4 was expressed in 293T cells and purified (Fig. 3a). As reported with the C-terminal domain of mouse EYA3 (ref. 6), EYA4 showed tyrosine-phosphatase activity with an artificial peptide under acidic conditions (pH 6.0). Its threonine-phosphatase was potentiated under basic pH, with an optimum pH of around 8.0 (Fig. 3b). The tyrosine-phosphatase required bivalent cations (Mg^{2+} or Mn^{2+}) (Fig. 3c), and $ZnCl_2$ (1 mM) and EDTA (5 mM) inhibited this activity (Supplementary Fig. 5). On the other hand, the threonine-phosphatase did not require a metal ion (Fig. 3d), and was not inhibited by 10 mM EDTA or EGTA (data not shown), but $ZnCl_2$ inhibited its activity (Fig. 3d). NaF inhibited both the tyrosine- and threonine-phosphatases, whereas calyculin and okadaic acid inhibited the threonine-phosphatase but not the tyrosine-phosphatase activity (Fig. 3e, f). Under optimal conditions, the K_m and K_{cat} were similar between tyrosine- and threonine-phosphatases, and they were comparable to those for protein phosphatase 2A, protein phosphatase 2B, and protein phosphatase 2C (Supplementary Fig. 6). Other mouse EYA family members, produced in 293T cells (Supplementary Fig. 7), also showed both tyrosine- and threonine-phosphatase activity (Supplementary Fig. 8). None of the members showed phosphatase activity against phosphorylated peptides of (pS)EEEEE and (pT)EEEEE, confirming that EYAs are not acid or alkaline phosphatases. The threonine-phosphatase activities of mouse EYA3 and EYA4 were confirmed by preparation in the wheat-germ cell-free system (Supplementary Fig. 9).

The tyrosine-phosphatase activity of the EYA proteins was previously assigned to the haloacid dehalogenase (HAD) domain in the C-terminal half[6,7]. Although its N-terminal domain is less well conserved, an alignment of the amino acid sequences revealed a conserved motif (Supplementary Fig. 10) in which six tyrosine residues are well conserved. We produced three EYA4 mutants: DYY, Y4 and D352N (Fig. 4a, b). For DYY, Ala was substituted for Asp 246, Tyr 247 and Tyr 250, and for Y4, Ala was substituted for Tyr 258, Tyr 261, Tyr 262 and Tyr 267; for D352N, Asn was substituted for Asp 352. As reported[6,7], Asp352Asn lost its tyrosine-phosphatase activity (Fig. 4c), but its threonine-phosphatase activity was unaffected (Fig. 4d). The tyrosine-phosphatase activity of DYY and Y4 was comparable to that of wild-type EYA4, but their threonine-phosphatase activity was severely affected, with Y4 showing the most disruption. This was also true with peptides from the C-terminal region of RNA polymerase II (Supplementary Fig. 11). When EYA3 was divided into an N-terminal and C-terminal domain, the C-terminal domain carried the tyrosine-phosphatase, but not the threonine-phosphatase, activity (Supplementary Fig. 12). In contrast, its N-terminal domain showed threonine-phosphatase activity, but negligible tyrosine-phosphatase activity. These results apparently contradict the previous report that assigned the threonine-phosphatase of EYA to the HAD domain[5]. When Asp352Asn and Y4 mutants were expressed in mouse fetal liver macrophages (Fig. 4e), Asp352Asn enhanced poly(I:C)-induced IFN-β expression as efficiently as the wild-type EYA4, whereas Y4 severely lost this ability (Fig. 4f). This was in contrast to the effect of the Y4 mutation on the ability of EYA4 to enhance the SIX4-mediated transcription of the myogenin gene promoter (Supplementary Fig. 13). The point mutations in the N or C termini did not affect its ability to interact with IPS-1 (Fig. 4g), suggesting that the threonine-phosphatase is critical for the ability of EYA4 to enhance the innate immune response.

Here we have reported that EYA4 interacts with IPS-1, STING and NLRX1, which are on the mitochondrial outer membrane or endoplasmic reticulum[15,18,19,21], and stimulates the IRF3-mediated transcription of the *Ifnb* and *Cxcl10* genes. A recent report indicates that EYA dephosphorylates a tyrosine residue of histone H2AX, and renders the cells resistant to genotoxic-agent-induced apoptosis[22]. These results indicate that EYA has dual functions: one to regulate the chromatin structure using its tyrosine-phosphatase, the other to

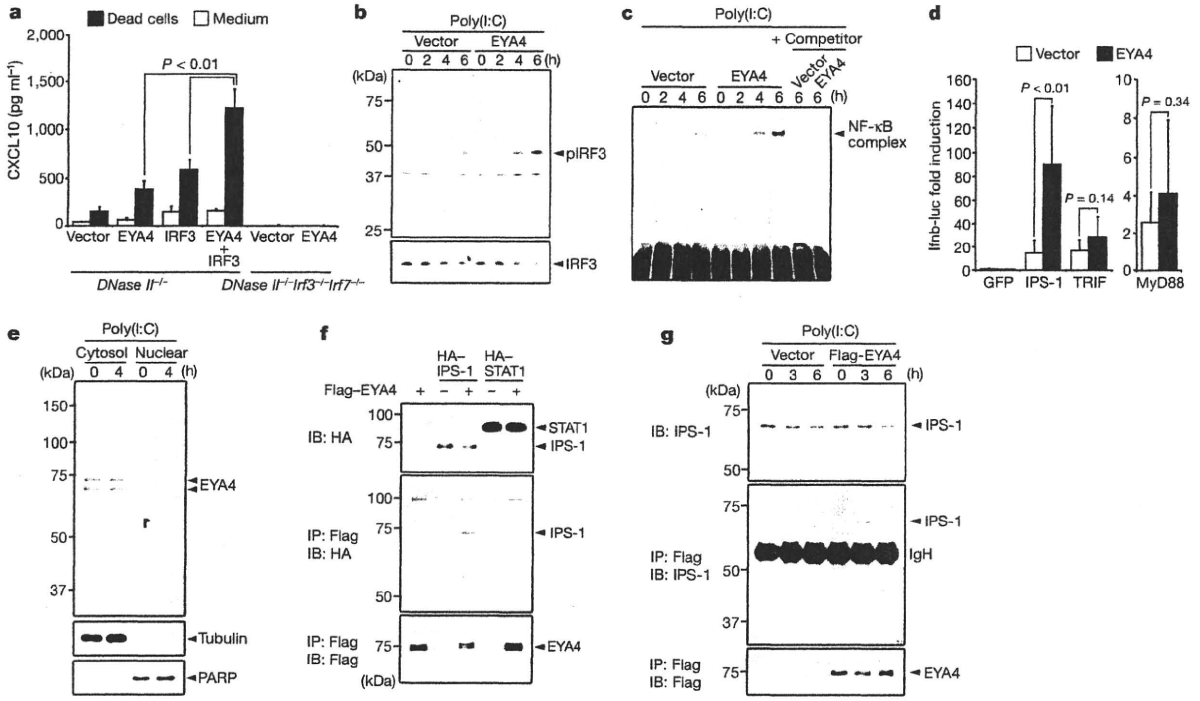

Figure 2 | Activation of the signalling cascade by EYA4. **a**, *DNase II*$^{-/-}$ or *DNase II*$^{-/-}$ *Irf3*$^{-/-}$ *Irf7*$^{-/-}$ MEFs expressing EYA4 and/or IRF3, were cultured with medium or dead cells, and CXCL10 levels were determined. **b**, **c**, MEFs containing vector control or EYA4 were transfected with 1 μg ml^{-1} poly(I:C) for the indicated times. The cell lysates were analysed by western blot for phosphorylated-IRF3 (pIRF3) (**b**), or nuclear extracts were analysed by electrophoretic mobility shift assays (EMSAs) for NF-κB (**c**). **d**, MEFs containing vector control or EYA4 were transfected with pGL3-Ifnb-luc, and pEF-EGFP, pEF-IPS-1, pEF-TRIF or pEF-MyD88. The luciferase activity is shown relative to the EGFP value. **e**, MEFs were treated with 1.0 μg ml^{-1} poly(I:C) for 4 h, and cell extracts were fractionated into cytoplasmic and nuclear fractions and analysed by western blotting. Two bands for EYA4 are probably due to alternative splicing[29]. The fractionation of the cell extracts was confirmed by blotting for tubulin and PARP. **f**, 293T cells were co-transfected with the vector for Flag–EYA4 and HA-tagged IPS-1 and STAT1. Cell lysates were immunoprecipitated (IP) with anti-Flag and analysed by western blotting. Cell lysates are shown at the top (5% of the input). IB, immunoblot. **g**, MEFs plus vector control or EYA4 were transfected with 1.0 μg ml^{-1} poly(I:C) for the indicated times. Cell lysates were immunoprecipitated with anti-Flag and analysed by western blotting. Cell lysates are shown at the top (10% of input). All error bars are s.d.

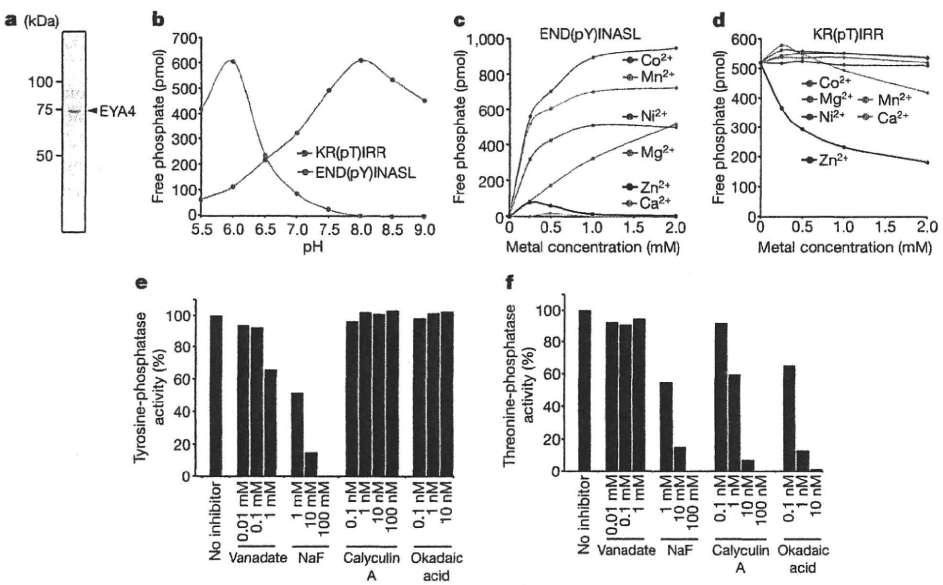

Figure 3 | Two different phosphatase activities in mouse EYA. **a**, Mouse EYA4 expressed in 293T, was purified and analysed by SDS–PAGE. **b–d**, Dephosphorylation with END(pY)INASL and 5 pmol EYA4 (**b**, **c**), or with KR(pT)IRR and 2.5 pmol EYA4 (**b**, **d**) at the indicated pH (**b**) or in the presence of metal ions (**c**, **d**) is shown. **e**, **f**, Dephosphorylation of RRLIEDAE(pY)AARG (**e**) or SDQEKRKQI(pT)VRGL (**f**) by 1.25 pmol EYA4 in the presence of phosphatase inhibitors is shown.

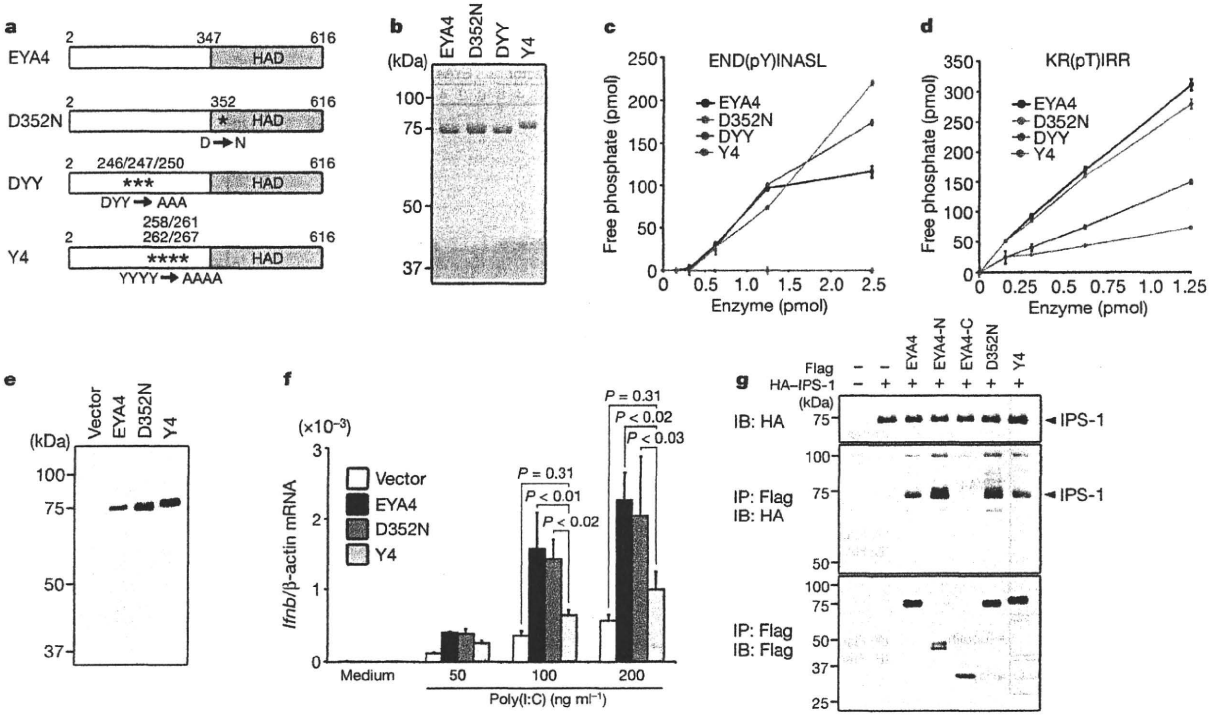

Figure 4 | The threonine-phosphatase activity of EYA4 is required for the innate immune reaction. a, Diagrams of EYA4 and its mutants are shown. **b**, EYA4 and its mutants, produced in 293T cells, were purified and analysed by SDS–PAGE. **c, d**, Dephosphorylation by EYA4 and its mutants is shown. **e, f**, Fetal liver macrophages were infected with EYA4 retrovirus. Cell lysates were analysed by western blot using an anti-Flag antibody (M2) (**e**). The cells were transfected with poly(I:C) for 6 h, and *Ifnb* mRNA levels were quantified relative to β-actin levels (**f**). **g**, 293T cells transfected with vectors for Flag–EYA4 or its mutants, and with HA–IPS-1. Cell lysates were immunoprecipitated (IP) with anti-Flag, followed by western blotting. Shown at the top is 10% of the input. All error bars are s.d.

regulate the innate immune response in the cytoplasm using its threonine-phosphatase. It will be interesting to study how the two phosphatase activities of EYA are regulated, and how the cellular localization of EYA is determined. The N-terminal region of EYA for the threonine-phosphatase had no apparent similarity with other phosphatases, yet its activity could be inhibited by okadaic acid. As found between protein phosphatase 1 and protein phosphatase 2A[23], the tertiary structure of the N-terminal domain of EYA may be similar to other threonine phosphatases. Several kinases (RIP1 (also known as RIPK1), IKK-ε (IKBKE), TBK1, IKK-α (CHUK) and IKK-β (IKBKB)) are involved in RIG-I–MDA5-mediated signal transduction[24]. It was previously proposed[25] that binding of viral RNA to RIG-I–MDA5 recruits signalling molecules (TRADD, TRAF3 and NEMO (IKBKG)), to form a large complex. It is possible that EYA is one of the components of this large complex, and regulates the signalling by modulating their phosphorylation state (Supplementary Fig. 14). Genes in the *EYA* family are often mutated in various autosomal-dominant disorders associated with branchial arch malformations, hearing loss, and ocular segment anomalies[26]. Mutations can be found throughout the EYA molecule[27], and some of these mutations have no effect on the tyrosine-phosphatase activity or on the interaction with a SIX family member[28]. Whether any of the mutations found in genes of the *EYA* family in human patients affect the threonine-phosphatase activity remains to be determined.

METHODS SUMMARY

Expression cloning. Double-stranded cDNA with poly(A) RNA from MEFs was inserted into a retroviral vector, and introduced into *E. coli* to generate a library (400 pools of 50 clones). Plasmid DNA from each pool was introduced into packaging cells, and the culture supernatant was used to infect *DNase II*$^{-/-}$ MEFs. The MEFs were allowed to engulf apoptotic *Cad*$^{-/-}$ thymocytes, and CXCL10 in the culture supernatant was quantified by ELISA. The positive pools were subjected to sib-selection.

Molecular biology, biochemistry and cell biology. Macrophages and MEFs were transformed by retrovirus-mediated transfection. Namalwa cells expressing mouse EYA4 were established by electroporation with EYA4 expression vector. The MFG-E8-mediated system was used for engulfment of apoptotic cells. The Fugene system was used to introduce nucleic acids into cells. IFN-β and CXCL10 were quantified by ELISA. The promoter activity of the *Ifnb* and myogenin genes was determined with Dual-Luciferase Reporter Assay System (Promega). Real-time PCR was performed using a LightCycler 480 system (Roche Diagnostics). The shRNA expression plasmids for human *EYA1*, *EYA2*, *EYA3* and *EYA4* were purchased from OriGene.

Production of recombinant EYAs. For recombinant EYA, the Flag-tag was ligated at the 5′ end of *Eya*, and inserted into the pEF-BOS vector. A point mutation was introduced by recombinant PCR. The expression vector was introduced into human 293T cells, and the recombinant protein was purified using anti-Flag M2 gel. In some cases, EYA was synthesized using the wheat-germ cell-free system, and purified.

Phosphatase assay. Phosphorylated synthetic peptides were custom-synthesized at the Toray Research Center, MBL, and Invitrogen. To assay the phosphatase activity, EYA was incubated with 400 μM phosphorylated peptide at 37 °C for 60 min, and released phosphate was quantified by a colourimetric method using malachite green-molybdate.

Statistical analysis. Results were statistically analysed using an analysis of variance (ANOVA) test.

Full Methods and any associated references are available in the online version of the paper at www.nature.com/nature.

Received 25 March; accepted 8 May 2009.
Published online 28 June; corrected 23 July 2009 (see full-text HTML version for details).

1. Meylan, E., Tschopp, J. & Karin, M. Intracellular pattern recognition receptors in the host response. *Nature* 442, 39–44 (2006).
2. Yoshida, H., Okabe, Y., Kawane, K., Fukuyama, H. & Nagata, S. Lethal anemia caused by interferon-β produced in mouse embryos carrying undigested DNA. *Nature Immunol.* 6, 49–56 (2005).
3. Kawane, K. *et al.* Chronic polyarthritis caused by mammalian DNA that escapes from degradation in macrophages. *Nature* 443, 998–1002 (2006).